



Petrogenesis and Ore Genesis of the Late Yanshanian Granites and Associated Porphyry-Skarn W-Mo Deposits from the Yunkai Area of South China: Evidence from the Zircon U-Pb Ages, Hf Isotopes and Sulfide S-Fe Isotopes

Xinyu Wang^{1,2}, Zhen Yang^{3*}, Nengsong Chen¹, Rui Liu³

1. School of Earth Sciences, China University of Geosciences, Wuhan 430074, China

2. Geological Prospecting Institute of Guangxi Zhuang Autonomous Region, Nanning 530023, China

3. Faculty of Earth Resources, China University of Geosciences, Wuhan 430074, China

 Xinyu Wang: <http://orcid.org/0000-0002-3359-1551>;  Zhen Yang: <http://orcid.org/0000-0003-0420-5516>

ABSTRACT: There are a wide range of magmatism and mineralization in the Yunkai area of South China during the Late Yanshanian Period, including the newly discovered Michang, Youmapo, San-chachong and Songwang porphyry-skarn W-Mo deposits. In this study, we obtained zircon U-Pb ages of the ore-bearing biotite granites and their mafic enclaves from 88 ± 1 to 110 ± 1 Ma. Zircons from the granites show Hf isotopic compositions with negative $\epsilon_{\text{Hf}}(t)$ values of -5.9 to -0.6 and calculated Hf model ages (T_{DM2}) of 1.5–1.2 Ga; indicating that the Middle Proterozoic crustal materials may have provided an important source for the magmatic rocks in this district during the Late Yanshanian Period, whereas zircons from the mafic enclaves show positive $\epsilon_{\text{Hf}}(t)$ values of 1.3 to 10.1 with younger Hf model ages (T_{DM2}) of 0.5–1.1 Ga, suggesting a mantle component may have involved in the granitic magma generation. Sulfur isotope study of the sulfide minerals from the W-Mo deposits show a narrow $\delta^{34}\text{S}$ distribution with most data ranging from -4.2‰ to 5.2‰. In addition, this study reports the first Fe isotopic compositions of pyrite in the W-Mo deposits, which show a uniform distribution range with the values near zero ($\delta^{56}\text{Fe}=0.16\text{‰}-0.58\text{‰}$, average 0.35‰; $\delta^{57}\text{Fe}=0.02\text{‰}-0.54\text{‰}$, average 0.48‰). These data indicate that the ore-forming materials may come from the deep-sourced granitic magma, and the mineralizations show a close relationship with the granitic magmatism during the Late Yanshanian Period. Combining with previous results, we suggest that there is a widespread porphyry-skarn W-Mo mineralization in the Yunkai area during the Late Cretaceous (80–110 Ma), which has a close relationship with the Late Yanshanian magmatism that may have formed during the rollback of the subducted Pacific Plate.

KEY WORDS: zircon U-Pb age, Hf isotopes, S-Fe isotopes, granitic magmatism, Late Yanshanian, Yunkai area.

0 INTRODUCTION

The South China Block has experienced a complicated tectono-magmatic-mineralization history during the Late Yanshanian Period, with widespread multiple-stage granitic rocks (Fig. 1a) and associated Cu-Au-Pb-Zn-Ag and W-Sn-Mo ore deposits (Li and Jiang, 2016; Li et al., 2016; Jiang et al., 2013; Mao et al., 2011, 2008; Yang et al., 2011; Li and Li, 2007; Zhou et al., 2006). It has become one of the most important tungsten mining areas in China or even in the world. Mao et al. (2008) put forward a three-stage formation model for

the South China tungsten deposits, namely, the Triassic (230–210 Ma), Jurassic (170–150 Ma) and Cretaceous (134–80 Ma) stages. It is noted that the Triassic tungsten mineralization is less important, with only a few tungsten-tin polymetallic deposits, such as those in the Gannan, Chongyi, and Dayu ore-concentrated areas in the Exian Tang tin-tungsten mineralization belt (Liu et al., 2008). The Jurassic metallogenesis is one of the most important metallogenic events in South China, and this time is also the main metallogenic period of tungsten. The main ore deposit types in this period include skarn-type and quartz-vein-type and a small amount of greisen-type. In recent years a large number of high-precision geochronology studies were carried out for this region's main tungsten-tin deposits and the ore-bearing granitic rocks, including the Shizhuyuan, Yaogangxian and Xintianling deposits in southern Hunan Province; the Taoxikeng, Dajinshan deposits in Jiangxi Province; the Shirenzhang deposit in northern Guangdong Province, and the Xin-

*Corresponding author: yangzhen@cug.edu.cn

© China University of Geosciences and Springer-Verlag GmbH Germany, Part of Springer Nature 2018

Manuscript received April 3, 2015.

Manuscript accepted December 10, 2016.

glu deposit in Fujian Province. Previous results showed that the major tungsten-tin mineralization took place between 165 and 150 Ma (Guo et al., 2012; Zhao et al., 2012, 2006; Chen M H et al., 2011; Fu et al., 2011; Chen F W et al., 2008; Jiang et al., 2008, 2006; Mao et al., 2008).

Yunkai area is a typical area in South China where devel-

oped Caledonian Orogeny (Wang et al., 2012, 2007), with widespread occurrence of Caledonian (Kwangian) granites (Fig. 1b). The Yanshanian mineralization is the most important metallogenic event in the Yunkai area, with important Ag-Au polymetallic mineralization of Early Yanshanian such as the Yakeng and Chengcu deposits; and the Pb-Zn-Au-Ag deposits

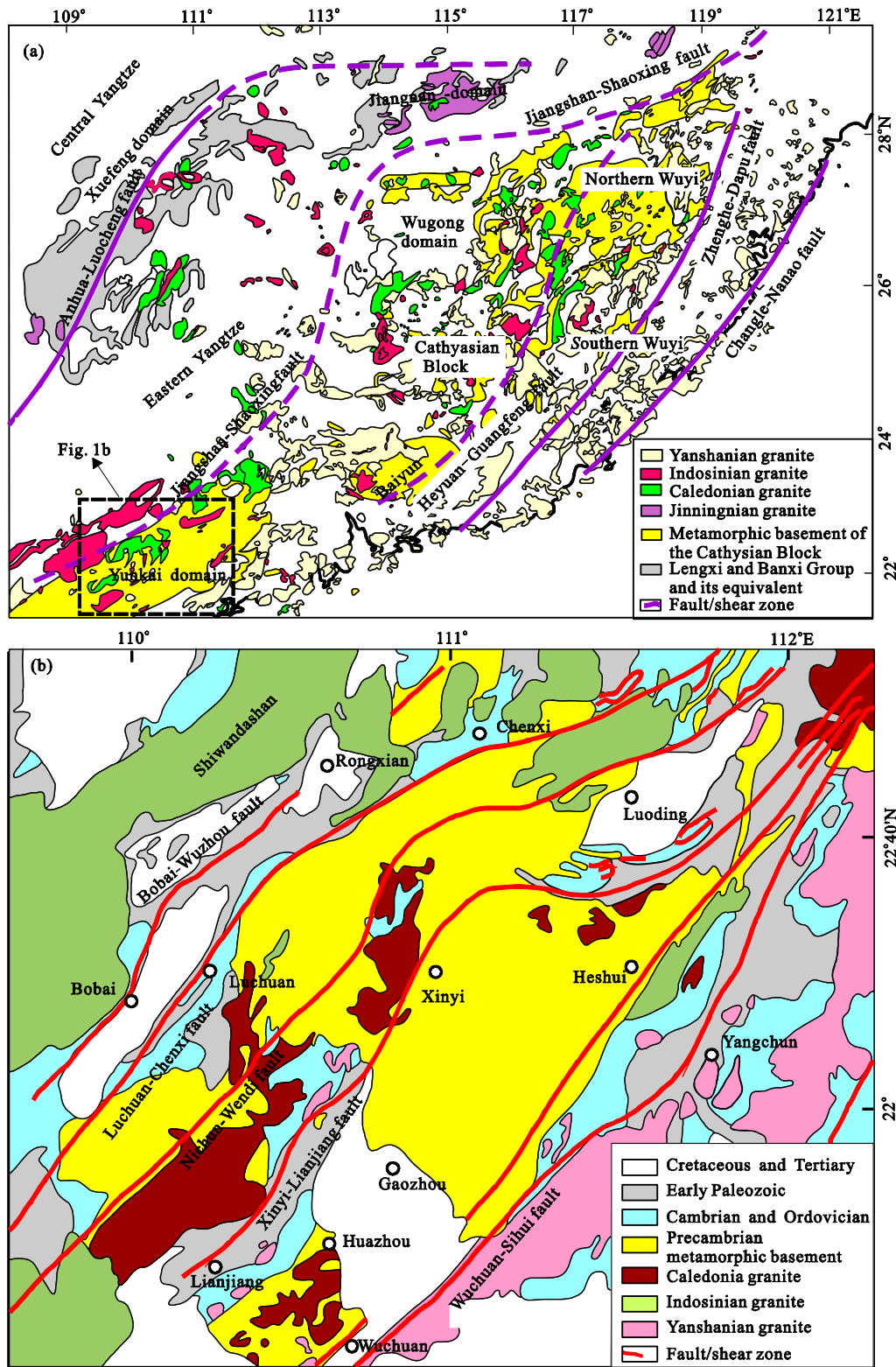


Figure 1. Simplified geological map showing the Yanshanian granitoids in the southeastern South China Block and the Precambrian basement in the Cathysia Block (a) and simplified geological map of the Yunkai area (b).

of Late Yanshanian such as the Fuzichong Pb-Zn-Ag deposit and the Jinshan Au deposit. In recent years, new tungsten-molybdenum (tin) deposits have been discovered in the Youmapo, Sanchachong, Michang, and Songwang (Fig. 2), which shows good potentials for tungsten-molybdenum ore prospecting in this region.

The tungsten-molybdenum deposits from the Yunkai area show large differences from the other parts of South China in the formation ages and their spatial distribution. In this region, the tungsten-molybdenum mineralization shows a close relationship to the large magmatic activity during the Late Yanshanian, in contrast to the Middle Yanshanian in other parts of South China (Yang et al., 2014). Therefore, the study of typical porphyry-skarn type tungsten-molybdenum deposits in the Yunkai area has important scientific significance to a better understanding of the Late Yanshanian magmatism and mineralization in the area.

In this study, we focus on the newly discovered Youmapo tungsten-molybdenum deposit, Sanchachong tungsten deposit, Michang tungsten-molybdenum deposit, Songwang tungsten tin (-molybdenum) deposit. On the basis of field geological investigation and petrography study, we carried out a detailed study of zircon U-Pb dating and Hf isotopes, and sulfide S-Fe isotope geochemistry, in an effort to reveal the ore deposit characteristics, fluid properties and the source of ore-forming materials. These data can provide further constraints on the spatial and temporal distribution patterns of the granitic magmatism and associated mineralization in South China during Late Yanshanian, and it will also provide a scientific basis for guiding future prospecting exploration in the region.

1 REGIONAL GEOLOGIC SETTING

Yunkai area is located in the southwest of South China Block (Fig. 1). Since the Early Paleozoic, the area was strongly influenced by the Caledonian Orogeny, Indosinian Orogeny and Yanshanian tectono-magmatic activity, with occurrence of granites in different ages and associated mineral deposits (Wang Y J et al., 2013, 2012, 2011; Zhang et al., 2012; Wan et al., 2010; Li Z X et al., 2009; Ling et al., 2006; Deng et al., 2004). As a result, the Yunkai area is not only located in the southwest of “Wu Yun” Caledonian orogenic belt in South China (Li et al., 2010), but also is located in the southwest of the famous “Qin Hang metallogenic belt” (Mao et al., 2011).

The Bobai-Cenxi fault and Wuchuan-Sihui fault divided the Yunkai area into three units, namely, the Southeast Guangxi, Yunkai and Middle Guangdong units. According to the characteristics of the rock assemblage and metamorphic deformation, the rocks of Yunkai area can be divided into two units: the upper part is mainly metamorphic volcanic-sedimentary formation with a set of greenschist facies (locally up to epidote-amphibolite facies), called the Yunkai Group; the lower part includes metamorphic rocks and intruded gneissic, ribbon, and eye (spot) ball shaped granitic rocks (including charnockite) up to amphibolite-granulite facies, which outcropped in Xinyi and Gaozhou area, known as Xinyi-Gaozhou complex rock (Wang et al., 2013; Chen et al., 2012; Peng et al., 2006). The lower lithology of Yunkai Group consists of mainly metamorphic arkose, mica-quartz schist, mica quartzite, garnet-mica-quartz schist, quartzite (siliceous rocks), with interbedded actinolite-diopside rock, metabasite (metagabbro, basalt and plagioclase amphibolite, etc.), banded magnetite layer, phosphate rock layer, and dolomitic marble layer. The lower unit of the Yunkai

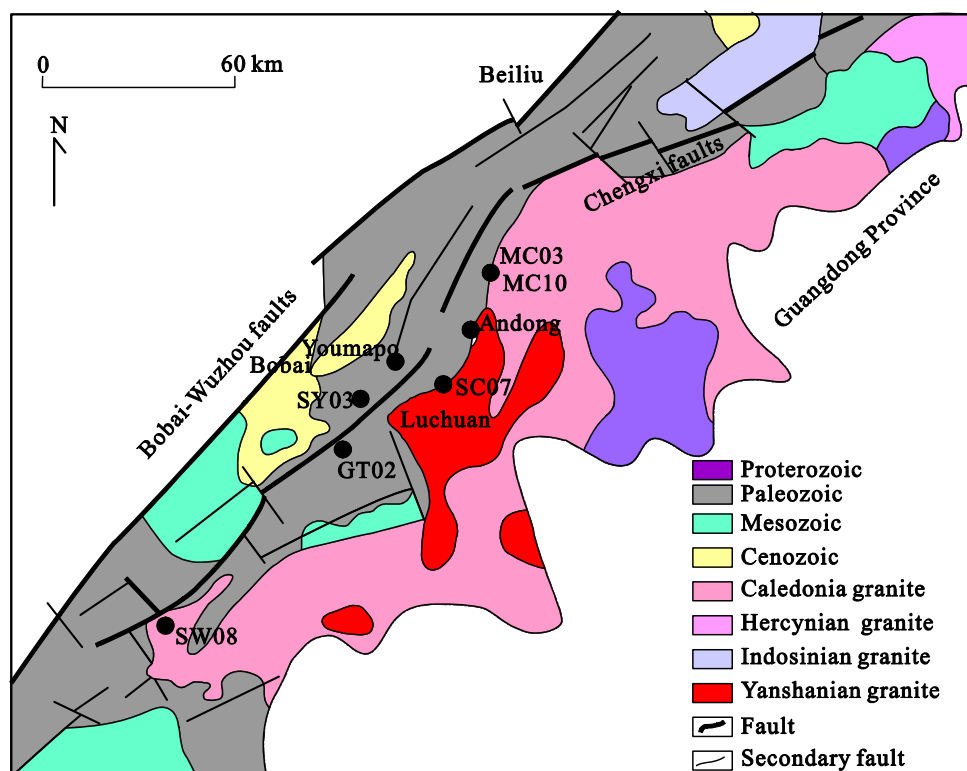


Figure 2. Geological map of the Yunkai area showing the distribution of W-Mo deposits.

Group has a thickness >1 307 m. The upper lithology of the Yunkai Group consists of mainly metamorphosed siltstone, quartz-sericite phyllite, siliceous rock, granet-bearing quartz schist, with thickness >1 343 m (Peng et al., 2006). In addition, there are a lot of Caledonian-to-Yanshanian Period granitic rocks distributed in the Yunkai area.

2 GEOLOGY OF THE PORPHYRY-SKARN DEPOSITS

The tungsten-molybdenum deposits in the Yunkai area are mainly located within the Bobai-Cenxi fault zone in the southeastern Guangxi Province, which belongs to the southern section of the Qin Hang metallogenic belt. This fault zone is also an important boundary fault, which separates Yunkai land to the southeast and the Bobai depression to the northwest (Zhou et al., 2015; GGST, 1986). As one of the important boundary faults in South China, this fault zone has experienced several tectonic movements and magmatic activities in the process of geologic evolution history. Since Caledonian Orogeny, this district has experienced multiple stage compression and extension. Especially during the Late Yanshanian stage occurred regional extension and large-scale magmatic activities with associated mineralization events, which formed a W-Mo-Sn-Pb-Zn-Ag polymetallic metallogenic belt (Mao et al., 2008; Chen et al., 1990). A number of large- and medium-sized skarn-type tungsten-molybdenum deposits occurred in the southwest segment of the fault zone, including the Youmapo tungsten-molybdenum deposit, the Andong tungsten-molybdenum deposit, the Sanchachong tungsten-molybdenum deposit, the Michang (Liusu, Mocun) tungsten-molybdenum deposit, and the Songwang tungsten-tin deposit (Tang, 2009; Zhong and Huang, 2007; Ye, 2005). All of these deposits have close relationship with granitic magmatism.

The Youmapo tungsten-molybdenum deposit is located in the northeast of Bobai County, about 20 km away from the Xiuling Village of Jingkou Town. The outcropped rocks include the Silurian and Devonian system formations in the mining area. The major thrust fracture in the mining area shows an NE-extending, with the secondary fault trending NW. The Youmapo granodioritic stock occurs in the southeast of the mining area, with an outcrop of about 1.3 km², which intruded into the Silurian and Devonian strata. Porphyritic and skarn mineralization occurred near the Youmapo granodioritic body and in the contact zone between the granodiorite and the host carbonate rock. The tungsten mineralization took place with the formation of skarn alteration. Part of the ore body formed within fractures of the granodioritic rock, with the form of molybdenite-quartz veins. The ore minerals include scheelite, molybdenite, bismuthinite, chalcopryrite, sphalerite, pyrite, marcasite, pyrrhotite and a small amount of wolframite and trace amount of natural gold. The gangue minerals are mainly garnet, quartz, calcite, fluorite; with minor amounts of actinolite, epidote, diopside, chlorite, plagioclase and white mica. The skarn minerals include garnet, diopside, actinolite, epidote, and chlorite. The alterations associated with the vein-type mineralization include mainly silicification, potassium alteration, chloritization, and sericitization.

The Sanchachong tungsten deposit is located in the southwest section of the Bobai-Wuzhou fault zone. This is

mainly a skarn-type tungsten deposit, which also contains minor molybdenum (Ye, 2005). The outcropped rocks in the mining area include the Ordovician and Devonian strata, including sandstone, limestone and argillaceous siltstone, which have all turned into schists during regional metamorphism. The major fault is the NE-trending compressive shear fault. Magmatic rock occurring in the mining area is mainly the biotite granite. Ore bodies are found mainly in the outer skarn contact zone in the Ordovician formation of the fourth period of Dongchong Group, which were controlled by fault. The shapes of the ore bodies include bedded and lenticular. Ore minerals include mainly scheelite, wolframite, pyrite, chalcopryrite, limonite, and cassiterite. The gangue minerals are quartz, chlorite, epidote, garnet, and mica. Alterations include skarnification, silicification, pyritization and greisenization.

The Michang tungsten-molybdenum deposit is located about 10 km from the Michang County. Ore bodies occur in the contact zone between the Michang granite and the Ordovician Huangai Group of marble, quartz schist, and gneiss. The Michang granitoid rocks of mainly biotite granite and granodiorite show a medium-coarse grained structure, which can be divided into two phases (internal phase and marginal phase). In the marginal facies, the phenomenon of hybrid can be seen. There are two major types of the ores, one is the tungsten-molybdenum ore associated with garnet skarn and the other is the tungsten ore associated with hornblende-epidote quartzite. Ore minerals include scheelite, molybdenite, pyrite and chalcopryrite. The gangue minerals are mainly of garnet, quartz, chlorite, calcite, hornblende, and epidote.

The Songwang tungsten-molybdenum-tin deposit in the Bobai Town is located in the southwest end of the Dongtao anticline, which is in the southeast of the Luchuan-Cenxi deep fault (Tang, 2009). The outcropped rocks include Early Palaeozoic migmatites and Middle-Lower Devonian low-grade metamorphic rocks. The fault systems in the mining area include mainly the SN-trending fault and secondarily the EW-trending fault. Magmatic rocks are widely distributed in the mining area, including mainly the Songwang fine-grained biotite granite and the Guogailing porphyritic granite.

Orebody occurs mainly within the Guogailing porphyritic granite and its contact zone with the augen migmatite in the layered and lenticular form. The orebody is mainly controlled by structural fractures of NE direction. The mineralization is mainly Mo, followed by W and Sn mineralization. Ore minerals include mainly molybdenite, followed by wolframite, cassiterite, pyrite, pyrrhotite, chalcopryrite, galena, sphalerite, columbite-tantalite, and ilmenite. The gangue minerals are plagioclase, potassium feldspar, quartz, biotite, sericite, white mica, and chlorite, with minor amounts of tourmaline and fluorite.

The alterations are mainly silicification, potassium feldspathization, greisenization, topazization, sericitization, followed by chloritization and pyritization. The silicification, potassium feldspathization and greisenization show a close relationship with the mineralization.

3 SAMPLE DESCRIPTION AND ANALYSIS METHOD

3.1 Sample Description

The studied samples are collected from four typical por-

phyry and skarn-type deposits including the Michang, Youmapo, Sanchachong, and Songwang in the western region of the Yunkai area. Five granite samples and one mafic enclave in the granite (Fig. 3) are used for zircon U-Pb age and Hf isotopic analysis (Fig. 4), and twelve samples of pyrite, pyrrhotite, galena and sphalerite are selected for S-isotope analysis (Fig. 7) and eleven pyrite samples are selected for Fe isotope analysis (Fig. 8).

Among them, samples MC03, MC10 and GT02 are col-

lected from the Michang tungsten-molybdenum deposit. Sample MC03 is a biotite granite, which consists mainly of potassium feldspar (~40%), plagioclase (~20%), quartz (~25%) and biotite (~10%). Accessory minerals include mainly magnetite, apatite, sphene and zircon. Sample MC10 is a mafic enclave in the Michang biotite granite, which shows a porphyritic structure and has a dioritic composition. The main minerals are plagioclase (~40%), potassium feldspar (~5%), quartz (~4%), hornblende (~35%), and biotite (~15%), with a small amount

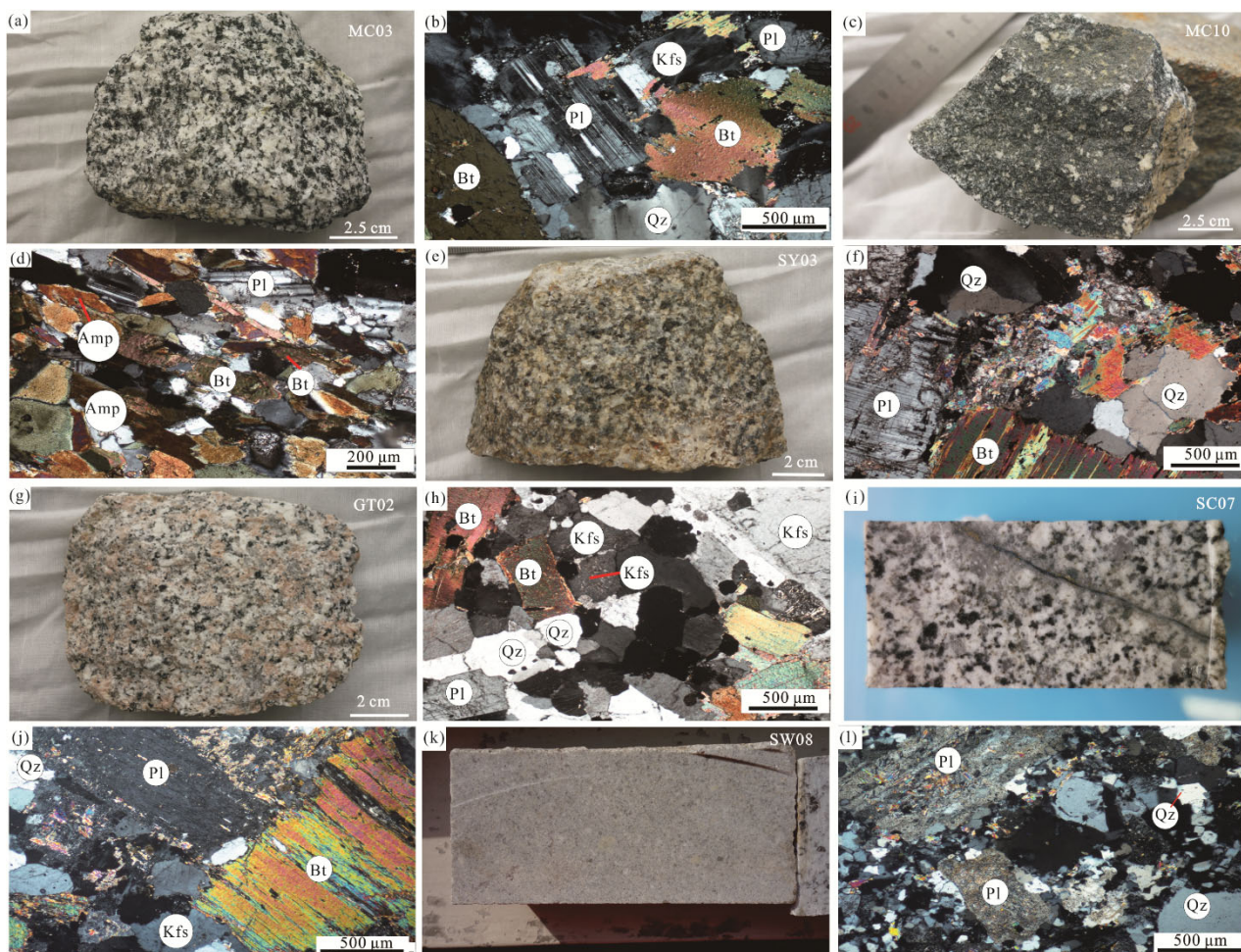


Figure 3. Field geological, sample and microscopic characteristics of the representative Late Yanshanian granites from the porphyry-skarn W-Mo deposits in the Yunkai area. Bt. biotite; Kfs. K-feldspar; Qz. quartz; Amp. amphibole; Pl. plagioclase.

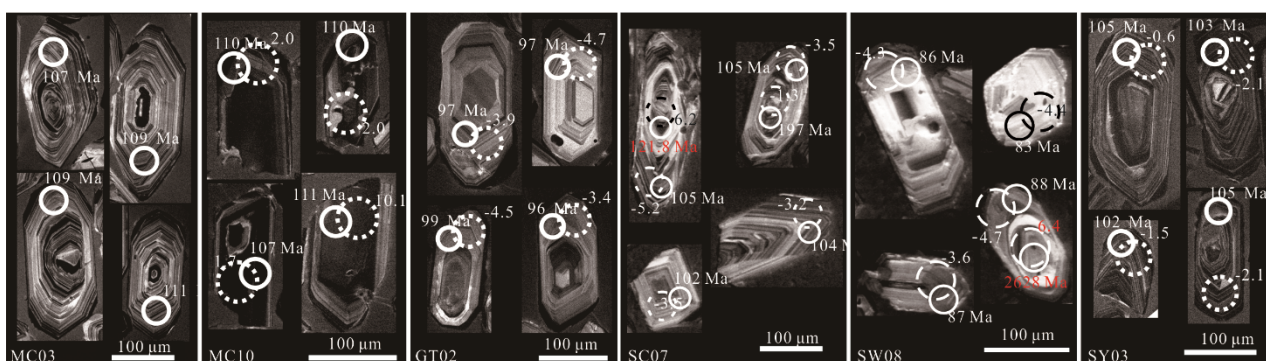


Figure 4. Representative cathodoluminescence (CL) images of zircons of granite samples from the porphyry-skarn W-Mo deposits in the Yunkai area. Round circles (solid line) with 32 μm diameter indicate the spots of LA-ICP-MS analyses with the $^{206}\text{Pb}/^{238}\text{U}$ age and spot numbers being labeled nearby.

of accessory minerals such as sphene, zircon and apatite (~1%). Sample GT02 is a biotite granite, consisting of potassium feldspar (~40%), plagioclase (~15%), quartz (~30%) and biotite (~10%). Accessory minerals include mainly apatite and zircon (a total of ~5%). Sample SY03 is a biotite granite from the Youmapo tungsten-molybdenum deposit, consisting of potassium feldspar (~42%), plagioclase (~23%), quartz (~25%) and biotite (~10%). Accessory minerals include apatite and zircon (a total of ~5%). Locally, chloritization occurred in this rock.

Sample SC07 is a biotite granite from the Sanchachong tungsten-molybdenum deposit. The main minerals are potassium feldspar (~40%), plagioclase (~18%), quartz (~32%) and biotite (~8%). Apatite, titanite and zircon (a total of ~2%) are mainly accessory minerals. Locally, chloritization also occurred in this rock.

Sample SW08 is a granite-porphry from the Songwang tungsten-molybdenum-(tin) deposit. The main minerals are potassium feldspar (~45%), plagioclase (~20%), quartz (~30%) and biotite (~3%). Apatite, titanite and zircon (a total of ~2%) are the main accessory minerals.

3.2 Methods

3.2.1 Zircon U-Pb age and Hf isotope

Zircon samples were separated using the method of heavy liquid and magnetic separation technology, and then hand-picked under a binocular microscope according to crystal shape, color and transparency. Selected zircon grains were mounted in an epoxy disc and polished to expose the interiors. The morphology and internal structure of zircons were characterized by optical microscopy and cathodoluminescence (CL) imaging using a Mono CL3+ (Gatan, USA) detection system in the Scanning Electron Microscopy Laboratory of Institute of Geology and Geophysics, Chinese Academy of Sciences, Beijing.

Zircon U-Pb isotope dating was completed in the State Key Laboratory of Geological Processes and Mineral Resources (GPMR) of China University of Geosciences (Wuhan) used LA-ICP-MS analysis method with GeoLas 2005 for Laser ablation system, Agilent 7500a for ICP-MS. Laser ablation process using helium as a carrier gas, argon as compensate gas to adjust the sensitivity, through a T-shape joint to mixture before them entering the ICP. Adding a small amount of nitrogen in the center of the plasma gases (Ar+He), can be effective to enhance the sensitivity, lower detection limit and improve the analysis precision (Hu et al., 2008a).

The resolution of analysis data includes about 20–30 s blank signal and 50 s sample signal in each time. Offline processing for the data analysis (including the selection of sample and the blank signal, the sensitivity drift correction, element content, U-Th-Pb isotope ratio and age calculation) using the software of ICPMSDataCal (Li et al., 2010; Liu et al., 2008). The detailed instrument operating conditions and the method of data processing are arranged according to Liu R et al. (2010). U-Pb isotope dating using isotopic fractionation of zircon standard 91500 as external standard calibration, two times 91500 analysis when each of five sample points analysis has been done. For U-Th-Pb isotope ratios drift related to the analysis time, using the way of linear interpolation of the 91500 changes for calibration (Li et al., 2010). U-Th-Pb isotope ratio

of the Zircon standard 91500 is in accordance with the recommended Wiedenbeck et al. (1995). Zircon sample's U-Pb age harmonic mapping and weighted average age calculation were completed by using Isoplot/Ex_ver3 (Ludwig, 2003).

The test of zircon Hf isotope ratios *in situ* micro zone by laser ablation of receiving more cups of plasma mass spectrometry (LA-MC-ICP-MS) was completed in the State Key Laboratory of Processes and Mineral Resources (GPMR), China University of Geosciences (Wuhan). The system of Laser ablation is GeoLas 2005 (Lambda Physik, Germany), the MC-ICP-MS is Neptune Plus (Thermo Fisher Scientific, Germany). The system is equipped with the signal smoothing device which is research independent and developed by laboratory. Even if the laser pulse frequency declines to 1 Hz, device still can obtain steady signal (Hu et al., 2012a). For the 100 and 93 nm laser, under the condition of a given instrument, using the helium as a carrier gas is two times higher than using the argon gas in signal sensitivity (Hu et al., 2008b). Research also suggests that the sensitivity of most elements can be further enhanced when it introduces a small amount of nitrogen (Hu et al., 2008a). Relative to the standard cone combination of Neptune Plus, a new design of X intercept cone combination and Jet sampling cone combination can improve the Hf, Yb and Lu sensitivity respectively 5.3 times, 4.0 times and 2.4 times under the condition of a small amount of nitrogen to joined. The laser output power can be adjusted, and the actual output energy density is 5.3 J/cm². Adopts the model is single point denudation, the spot beam fixed at 44 μm. Details of analysis method and conditions about instrument can refer to Hu et al. (2012b).

The major limitation to accurate *in situ* zircon Hf isotope determination by LA-MC-ICP-MS is the very large isobaric interference from ¹⁷⁶Yb and, to a much lesser extent ¹⁷⁶Lu on ¹⁷⁶Hf. Research shows that the quality of Yb fractionation factor (β_{Yb}) is not a fixed value in the process of testing for a long time. The β_{Yb} of the zircon Hf isotopic interference correction by testing in sample solution way does not apply to the laser sample pattern (Woodhead et al., 2004). The β_{Yb} error estimation will significantly affect ¹⁷⁶Yb interference correction to ¹⁷⁶Hf, and further affect ¹⁷⁶Hf/¹⁷⁷Hf ratio accurate determination. In this experiment, we obtained the zircon sample's β_{Yb} for interference correction. ¹⁷⁹Hf/¹⁷⁷Hf=0.732 5 and ¹⁷³Yb/¹⁷¹Yb=1.130 17 (Segal et al., 2003) were used to calculate the β_{Hf} and β_{Yb} quality fractionation factor of Hf and Yb. ¹⁷⁹Hf/¹⁷⁷Hf and ¹⁷³Yb/¹⁷¹Yb ratios were used to calculate Hf (β_{Hf}) and Yb (β_{Yb}) the quality of the deviation. Deduct ¹⁷⁶Yb commensuration ectopic interference to ¹⁷⁶Hf by using the ¹⁷⁶Yb/¹⁷³Yb=0.793 81 (Segal et al., 2003). Deduct the relatively small disturbance of ¹⁷⁶Lu commensuration ectopic interference to ¹⁷⁶Hf by using the ¹⁷⁶Lu/¹⁷⁵Lu=0.026 56 (Blichert-Toft et al., 1997).

As Yb and Lu have similar physical and chemical properties, we use the β_{Yb} quality fractionation factor of Yb to correct Lu quality fractionation behavior in this experiment. The analysis of data's off-line process was accomplished (including the sample and the blank signal selection, isotope quality fractionation correction) using software ICPMSDataCal (Liu X H et al., 2010), $\epsilon_{Hf}(t)$ was calculated with ¹⁷⁶Lu decay constant of $1.865 \times 10^{-11} \text{ a}^{-1}$ (Scherer et al., 2001), the

present-day chondritic ratios of $^{176}\text{Hf}/^{177}\text{Hf}=0.282\ 772$ and $^{176}\text{Lu}/^{177}\text{Hf}=0.033\ 2$ (Blichert-Toft et al., 1997). Hf model age (T_{DMI}) of depleted mantle calculated using current depleted mantle $^{176}\text{Hf}/^{177}\text{Hf}=0.283\ 25$ and $^{176}\text{Lu}/^{177}\text{Hf}=0.038\ 4$ (Griffin et al., 2000). Hf model age (T_{DM2}) of the two-phase calculated using an average of continental crust $^{176}\text{Lu}/^{177}\text{Hf}=0.015$ (Griffin et al., 2002).

3.2.2 Sulfide S and Fe isotopes

Pyrite and pyrrhotite are predominant sulfide minerals accompanied with the W-Mo mineralization, and were collected in the Sanchachong, Songwang and Sanyu deposits, to analyze the sulfide sulfur isotopic ($n=11$) and iron isotopic ($n=12$) geochemistry. S isotope test was accomplished at the Isotope Laboratory University of Arizona in the United States (Environmental Isotope Laboratory, University of Arizona). Samples after crushing, oscillation, washing one hour and drying in the ultrasonic cleaning machine, differently selected sulfide mineral grains 0.5 g of pyrite, pyrrhotite, galena and sphalerite under the binocular microscope. Pyrite and other sulfides heating to 1 150 °C under the condition of high vacuum, SO_2 were extracted with Cu_2O as oxidant, frozen the release of SO_2 with liquid nitrogen into the charge for mass spectrometry analysis. Isotope values expression with the ratio micrometer difference of sample (A) and the corresponding standard R, says that $\delta M_A = [(R_A - R_{\text{Std}}) / R_{\text{Std}}] \times 100$ (type of $R = (\text{S}^{34} / \text{S}^{32})$; $M = \text{S}^{34}$; R_{Std} is the reference standard ratio, sulfur isotope standard using V-CDT). Average analysis error of delta value, sulfur is $\pm 0.2\%$. The test of Fe isotope work accomplishes in Center of the Water Environment of Canada Trent University (Water Quality Centre, Trent University, Canada).

4 RESULTS

4.1 U-Pb Ages

4.1.1 Michang biotite granites and mafic enclaves

Zircon grains are mostly colorless and transparent in Sample MC03 of Michang biotite granite, part is dark brown. The size of zircon grains ranges in 50–300 μm , and the length to width ratios are between 1 : 1 and 5 : 1. In the cathodoluminescence (CL) images (Fig. 4, MC03), almost all the zircons show typical rhythmic oscillation zoning, indicating magmatic origin. In addition, small amounts of zircons show obvious core-rim structures. According to the U-Pb dating of eighteen zircon grains of MC03 (Table 1, Fig. 5, MC03), the $^{206}\text{Pb}/^{238}\text{U}$ ages are between 107 and 113 Ma, with a weighted mean $^{206}\text{Pb}/^{238}\text{U}$ age of 110 ± 1 Ma (MSWD=2.0), and this age may represent the emplacement age of the Michang biotite granite. In sample MC10 of the mafic enclaves in the biotite granite, zircon grains are mostly colorless and transparent, and part is tan. The grain size ranges in 30–200 μm , and the length to width ratios are between 1 : 1 and 5 : 1. In the cathodoluminescence (CL) images (Fig. 4, MC10), most zircon grains display patch-shaped band, planar band or band, and a handful of zircon grains show rhythmic oscillation zoning. In addition, small amounts of zircon grains show also core-rim structures. Fourteen zircon U-Pb dating results yield $^{206}\text{Pb}/^{238}\text{U}$ ages between 106 and 112 Ma, with a weighted mean $^{206}\text{Pb}/^{238}\text{U}$ age of 109 ± 1 Ma (MSWD=1.8) (Table 1, Fig. 5, MC10). A spot analysis also points to an inherited zircon in this sample with a $^{206}\text{Pb}/^{238}\text{U}$ age of 194 ± 6 Ma.

In Sample GT02, zircon grains are mostly colorless, transparent or translucent, and a part is light brown. The grain size ranges in 50–300 μm , and the length to width ratios are between 1 : 1 and 4 : 1. In the cathodoluminescence (CL) images (Fig. 4, GT02), almost all the zircons show typical rhythmic

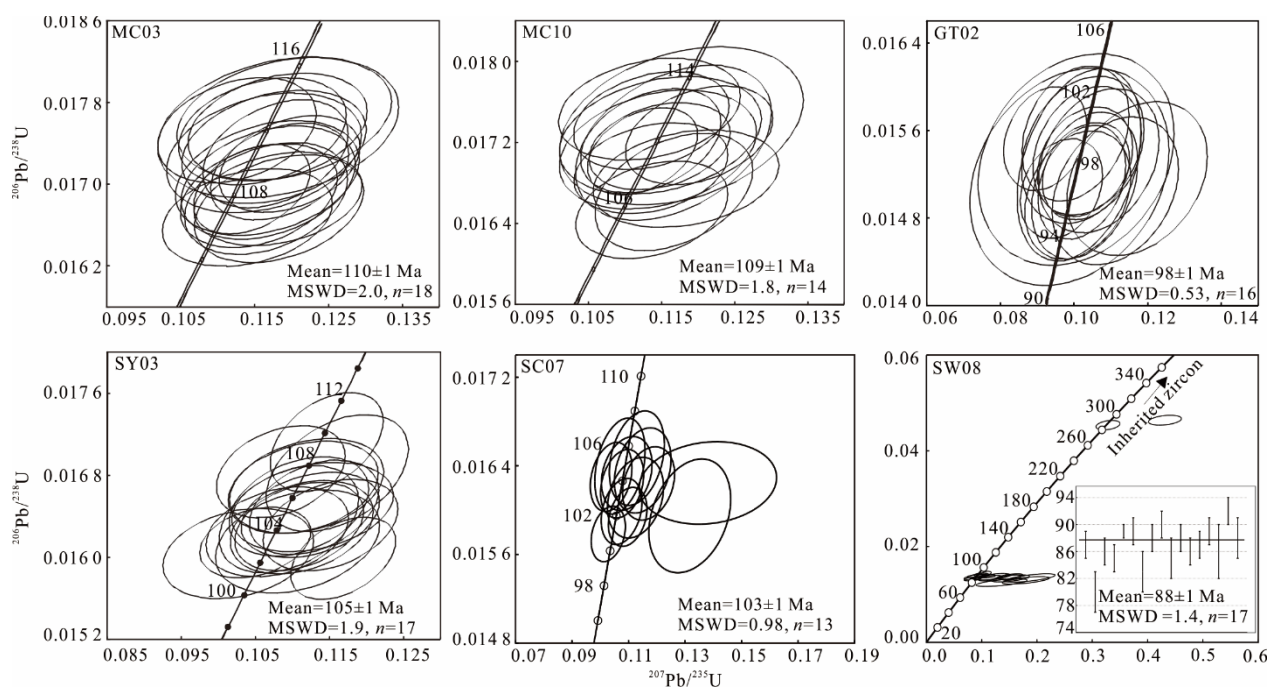


Figure 5. Concordia diagrams of LA-ICP-MS zircon U-Pb data from granite samples from the porphyry-skarn W-Mo deposits in the Yunkai area.

oscillation zoning, indicating magmatic origin. Sixteen zircon grains yielded a weighted mean $^{206}\text{Pb}/^{238}\text{U}$ age of 98 ± 1 Ma (MSWD=0.5) (Table 1, Fig. 5, GT02).

4.1.2 Youmapo biotite granite

In Sample SY03, the Youmapo biotite granite, zircon grains are mostly colorless, transparent or translucent, and a part is brown. The size ranges in 50–250 μm , and the length to width ratios are between 1 : 1 and 3 : 1. In the cathodoluminescence (CL) images (Fig. 4, SY03), almost all the zircons show typical rhythmic oscillation zoning, indicating magmatic origin. Seventeen zircon grains yielded a weighted mean $^{206}\text{Pb}/^{238}\text{U}$ age of 105 ± 1 Ma (MSWD=1.9) (Table 1, Fig. 5, SY03).

4.1.3 Sanchachong biotite granite

In Sample SC07, the Sanchachong biotite granite, zircon grains are mostly colorless, transparent or translucent. The grain size ranges in 30–300 μm , and the length to width ratios are between 1 : 1 and 4 : 1. In the cathodoluminescence (CL) images (Fig. 4, SC07), almost all the zircons show typical rhythmic oscillation zoning, indicating magmatic origin. Fifteen zircon grains yielded a weighted mean $^{206}\text{Pb}/^{238}\text{U}$ age of 103 ± 1 Ma (MSWD=0.98) (Table 1, Fig. 5, SC07). Two analyses point to inherited zircons, showing $^{206}\text{Pb}/^{238}\text{U}$ ages of 197 ± 9 and $1\,218\pm 72$ Ma.

4.1.4 Songwang granite

In Sample SW08 of the Songwang granite, zircon grains are mostly colorless, transparent or translucent. The grain size ranges in 40–300 μm , and the length to width ratios are between 1 : 1 and 5 : 1. In the cathodoluminescence (CL) images (Fig. 4, SW08), almost all the zircons show typical rhythmic oscillation zoning, indicating magmatic origin.

Twenty zircon grains yielded a weighted mean $^{206}\text{Pb}/^{238}\text{U}$ age of 88 ± 1 Ma (MSWD=1.4) (Table 1, Fig. 5, SW08). Three analyses also point to inherited zircons, showing $^{206}\text{Pb}/^{238}\text{U}$ ages of 286 ± 4 , 292 ± 4 and $2\,628\pm 54$ Ma.

4.2 Hf Isotopic Compositions

On the basis of the U-Pb age, we choose five samples for the zircon Hf isotopic analyses. The results are listed in Table 2. Fourteen magmatic zircons from the mafic enclaves of Sample MC10 show significantly higher $^{176}\text{Hf}/^{177}\text{Hf}$ ratio than those zircons from the biotite granite (Sample MC02), with $\varepsilon_{\text{Hf}}(t)$ values range from 1.3 to 10.1 when calculated at $t=109$ Ma, and the corresponding two-stage depleted mantle Hf model ages (T_{DM2}) range from 521 to 1 085 Ma (Figs. 6a, 6b).

Sixteen magmatic zircons from Sample GT02 granite samples show a relatively uniform range of $\varepsilon_{\text{Hf}}(t)$ values from -5.9 to -3.1 when calculated at $t=105$ Ma, and the corresponding two-stage depleted mantle Hf model age (T_{DM2}) ranges from 1 355 to 1 534 Ma (Figs. 6c, 6d).

Sixteen magmatic zircons from Sample SY03 granite samples show a relatively uniform range of $\varepsilon_{\text{Hf}}(t)$ values from -2.5 to -0.6 when calculated at $t=105$ Ma, the corresponding two-stage depleted mantle Hf model age (T_{DM2}) ranges from 521 to 1 085 Ma (Figs. 6e, 6f).

Thirteen magmatic zircons from Sample SC07 show a small $\varepsilon_{\text{Hf}}(t)$ range from -5.2 to -2.0 when calculated at $t=103$ Ma, and the

corresponding two-stage depleted mantle Hf model age (T_{DM2}) ranges from 1 334 to 1 494 Ma. Two detrital zircon cores (197 and 1 218 Ma) show $\varepsilon_{\text{Hf}}(t)$ values of -1.3 and 6.2, and the calculated T_{DM2} ages are 1 314 and 1 628 Ma (Figs. 6g, 6h).

Fourteen magmatic zircons from Sample SW08 show $\varepsilon_{\text{Hf}}(t)$ values of -5.2 to -3.6 when calculated at $t=88$ Ma, and the corresponding two-stage depleted mantle Hf model ages (T_{DM2}) range from 1 381 to 1 482 Ma (Figs. 6i, 6j). One detrital zircon

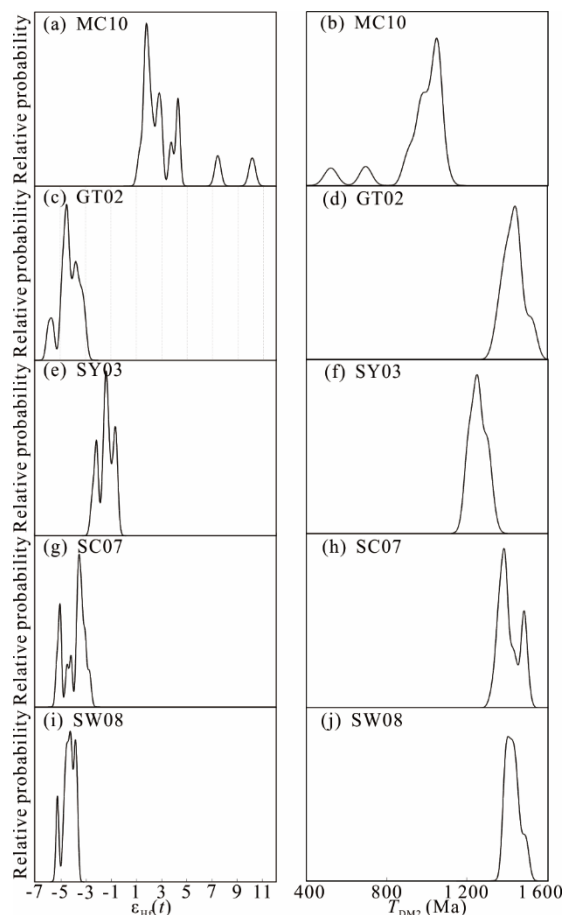


Figure 6. Zircon $\varepsilon_{\text{Hf}}(t)$ values and two-stage Hf model ages (T_{DM2}) for granite samples from the porphyry-skarn W-Mo deposits in the Yunkai area.

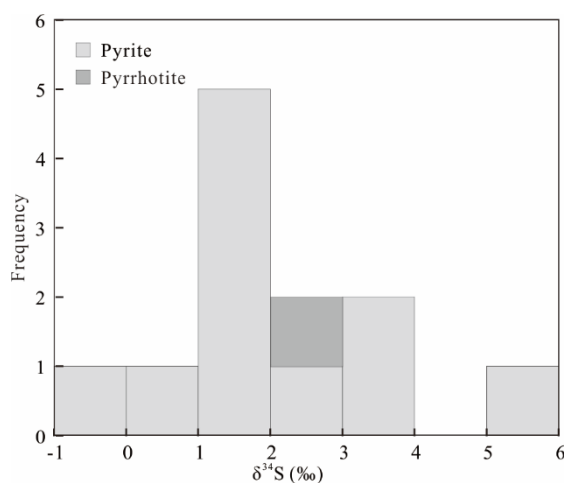


Figure 7. $\delta^{34}\text{S}$ histograms of sulfides from the porphyry-skarn W-Mo deposits in the Yunkai area.

Table 1 LA-ICP-MS U-Pb data for zircons from the Late Yanshanian granites from the porphyry-skarn W-Mo deposits in the Yunkai area

Point	Th (μg/g)	U (μg/g)	Th/U	²⁰⁷ Pb/ ²⁰⁶ Pb	1σ	²⁰⁷ Pb/ ²³⁵ U	1σ	²⁰⁶ Pb/ ²³⁸ U	1σ	²⁰⁷ Pb/ ²⁰⁶ Pb	1σ	²⁰⁷ Pb/ ²³⁵ U	1σ	²⁰⁶ Pb/ ²³⁸ U	1σ
MC03															
1	418	798	0.52	0.0494	0.0020	0.1140	0.0047	0.0167	0.0002	169	92	110	4	107	1
2	370	638	0.58	0.0491	0.0016	0.1178	0.0040	0.0173	0.0002	154	78	113	4	111	1
3	538	1251	0.43	0.0497	0.0016	0.1184	0.0038	0.0171	0.0002	189	74	114	3	109	1
4	489	607	0.81	0.0500	0.0019	0.1165	0.0045	0.0169	0.0002	195	89	112	4	108	1
5	408	632	0.65	0.0497	0.0022	0.1167	0.0051	0.0171	0.0002	189	104	112	5	109	1
6	333	556	0.60	0.0484	0.0026	0.1182	0.0067	0.0176	0.0003	117	122	113	6	112	2
7	485	734	0.66	0.0487	0.0022	0.1163	0.0054	0.0173	0.0002	200	109	112	5	111	2
8	336	611	0.55	0.0513	0.0021	0.1183	0.0047	0.0168	0.0002	254	88	114	4	107	1
9	246	517	0.48	0.0500	0.0021	0.1169	0.0048	0.0170	0.0002	195	94	112	4	109	1
10	404	742	0.54	0.0497	0.0019	0.1156	0.0043	0.0169	0.0002	189	89	111	4	108	1
11	1061	1266	0.84	0.0489	0.0013	0.1146	0.0032	0.0170	0.0002	143	66	110	3	108	1
12	320	675	0.47	0.0489	0.0020	0.1181	0.0049	0.0176	0.0002	143	96	113	4	112	1
13	266	524	0.51	0.0491	0.0024	0.1190	0.0059	0.0176	0.0002	150	115	114	5	113	2
14	366	662	0.55	0.0483	0.0019	0.1160	0.0046	0.0175	0.0002	122	94	111	4	112	1
15	370	611	0.61	0.0510	0.0020	0.1182	0.0046	0.0169	0.0002	239	91	113	4	108	1
16	295	536	0.55	0.0466	0.0018	0.1126	0.0044	0.0175	0.0002	28	89	108	4	112	1
17	453	752	0.60	0.0501	0.0016	0.1197	0.0039	0.0172	0.0002	198	105	115	4	110	1
18	344	521	0.66	0.0489	0.0020	0.1176	0.0051	0.0174	0.0002	139	96	113	5	111	1
MC10															
1	289	665	0.43	0.0502	0.0022	0.1166	0.0055	0.0172	0.0003	211	102	112	5	110	2
2	286	494	0.58	0.0508	0.0023	0.1183	0.0052	0.0168	0.0002	232	104	114	5	108	1
3	324	584	0.56	0.0503	0.0017	0.1201	0.0041	0.0173	0.0002	209	80	115	4	110	1
4	359	545	0.66	0.0511	0.0021	0.1167	0.0044	0.0167	0.0002	243	99	112	4	107	1
5	191	432	0.44	0.0487	0.0023	0.1145	0.0055	0.0171	0.0002	132	115	110	5	110	2
6	717	881	0.81	0.0503	0.0018	0.1137	0.0043	0.0165	0.0002	209	88	109	4	106	1
7	284	364	0.78	0.0489	0.0024	0.1148	0.0056	0.0173	0.0002	143	117	110	5	110	2
8	1662	1348	1.23	0.0471	0.0017	0.1136	0.0043	0.0174	0.0002	54	89	109	4	111	1
9	203	314	0.65	0.0497	0.0030	0.1177	0.0068	0.0174	0.0003	189	141	113	6	111	2
10	247	517	0.48	0.0471	0.0022	0.1133	0.0051	0.0175	0.0002	58	107	109	5	112	1
11	513	916	0.56	0.0482	0.0017	0.1147	0.0040	0.0172	0.0002	109	77	110	4	110	1
12	576	860	0.67	0.0480	0.0017	0.1135	0.0039	0.0172	0.0002	98	88	109	4	110	1
13	575	671	0.86	0.0485	0.0019	0.1136	0.0043	0.0169	0.0002	124	91	109	4	108	1
14	3394	2239	1.52	0.0473	0.0013	0.1124	0.0031	0.0171	0.0002	65	63	108	3	109	1

Table 1 Continued

Point	Th ($\mu\text{g/g}$)	U ($\mu\text{g/g}$)	Th/U	$^{207}\text{Pb}/^{206}\text{Pb}$	$^{207}\text{Pb}/^{235}\text{U}$	$^{206}\text{Pb}/^{238}\text{U}$	$^{207}\text{Pb}/^{206}\text{Pb}$	$^{207}\text{Pb}/^{235}\text{U}$	$^{206}\text{Pb}/^{238}\text{U}$	$^{207}\text{Pb}/^{235}\text{U}$	$^{206}\text{Pb}/^{238}\text{U}$
					1σ	1σ	1σ	1σ	1σ	1σ	1σ
SC07											
1	304	2.358	0.13	0.0517	0.0026	0.1171	0.0061	0.0162	0.0002	112	104
2	618	1.851	0.33	0.0500	0.0030	0.1130	0.0064	0.0165	0.0003	109	105
3c	358	1.367	0.26	0.0563	0.0026	0.2567	0.0174	0.0310	0.0015	232	197
4	543	4.737	0.11	0.0470	0.0019	0.1028	0.0040	0.0158	0.0002	99.4	101
5	200	920	0.22	0.0606	0.0043	0.1317	0.0096	0.0160	0.0003	126	102
6	582	1.951	0.3	0.0512	0.0031	0.1125	0.0065	0.0161	0.0002	108	103
7	897	3.178	0.28	0.0494	0.0023	0.1076	0.0048	0.0160	0.0002	104	102
8	612	3.327	0.18	0.0497	0.0021	0.1097	0.0045	0.0159	0.0002	106	102
9	624	2.638	0.24	0.0488	0.0027	0.1094	0.0059	0.0163	0.0002	105	104
10	1.185	2.505	0.47	0.0464	0.0022	0.1039	0.0049	0.0163	0.0002	100	104
11	783	2.797	0.28	0.0482	0.0023	0.1077	0.0050	0.0162	0.0002	104	104
12	532	2.541	0.21	0.0475	0.0027	0.1070	0.0059	0.0164	0.0003	103	105
13c	383	384	1	0.0808	0.0030	2.2548	0.0808	0.2011	0.0025	1198	1181
14	338	1.858	0.18	0.0514	0.0031	0.1150	0.0066	0.0164	0.0003	111	105
15	357	1.279	0.28	0.0611	0.0068	0.1381	0.0161	0.0163	0.0003	131	104
SW08											
1	151	241	0.63	0.1007	0.0136	0.1798	0.0282	0.0130	0.0005	168	83
2c	416	2.011	0.21	0.0526	0.0022	0.3285	0.0144	0.0454	0.0007	288	286
3	393	683	0.58	0.0624	0.0063	0.1152	0.0134	0.0134	0.0004	111	86
4	302	498	0.61	0.0795	0.0071	0.1506	0.0156	0.0138	0.0004	142	88
5	215	393	0.55	0.0824	0.0111	0.1516	0.0231	0.0133	0.0005	143	85
6	200	246	0.82	0.1013	0.0136	0.1877	0.0299	0.0134	0.0006	175	86
7	1.132	961	1.18	0.0461	0.0053	0.0844	0.0106	0.0133	0.0003	82	85
8	285	463	0.61	0.0903	0.0067	0.1521	0.0122	0.0135	0.0004	144	87
9	416	684	0.61	0.0600	0.0089	0.1115	0.0176	0.0135	0.0003	107	86
10	1.661	1.062	1.56	0.0557	0.0030	0.1079	0.0062	0.0144	0.0003	104	92
11	1.199	956	1.25	0.0467	0.0063	0.0876	0.0129	0.0136	0.0004	85	87
12	166	257	0.65	0.0793	0.0158	0.1362	0.0305	0.0125	0.0005	130	80
13	301	458	0.66	0.0637	0.0099	0.1203	0.0207	0.0137	0.0005	115	88
14	2.377	1.283	1.85	0.0472	0.0053	0.0902	0.0113	0.0139	0.0003	88	89
15c	172	655	0.26	0.0671	0.0029	0.4315	0.0197	0.0464	0.0007	220	292
16c	958	1.281	0.75	0.0671	0.0032	0.4315	0.0197	0.0464	0.0007	364	2098
17	1.326	970	1.37	0.0466	0.0045	0.0887	0.0095	0.0138	0.0003	86	88
18	2.165	1.300	1.67	0.0517	0.0045	0.0994	0.0088	0.0141	0.0003	96	90
19	1.392	952	1.46	0.0566	0.0055	0.1083	0.0108	0.0139	0.0003	104	89
20	151	241	0.63	0.1007	0.0136	0.1798	0.0282	0.0130	0.0005	168	83

Table 1 Continued

Point	Th (μg/g)	U (μg/g)	Th/U	²⁰⁷ Pb/ ²⁰⁶ Pb	1σ	²⁰⁷ Pb/ ²³⁵ U	1σ	²⁰⁶ Pb/ ²³⁸ U	1σ	²⁰⁷ Pb/ ²⁰⁶ Pb	1σ	²⁰⁷ Pb/ ²³⁵ U	1σ	²⁰⁶ Pb/ ²³⁸ U	1σ
SY03															
1	355	1.398	0.25	0.0494	0.0017	0.1124	0.0038	0.0164	0.0002	169	84	108	3	105	1
2	197	1.132	0.17	0.0491	0.0015	0.1109	0.0035	0.0163	0.0002	154	77	107	3	104	1
3	126	869	0.14	0.0464	0.0019	0.1027	0.0042	0.0160	0.0002	20	100	99	4	103	1
4	161	1.044	0.15	0.0512	0.0017	0.1151	0.0037	0.0163	0.0002	256	74	111	3	104	1
5	600	1.974	0.30	0.0529	0.0013	0.1168	0.0029	0.0160	0.0002	328	28	112	3	102	1
6	148	926	0.16	0.0488	0.0018	0.1119	0.0042	0.0167	0.0002	200	89	108	4	107	1
7	216	1.204	0.18	0.0489	0.0018	0.1095	0.0038	0.0164	0.0002	143	90	106	4	105	1
8	195	1.320	0.15	0.0483	0.0017	0.1080	0.0039	0.0162	0.0002	122	81	104	4	104	1
9	301	1.079	0.28	0.0495	0.0017	0.1113	0.0039	0.0163	0.0002	169	78	107	4	104	1
10	201	1.206	0.17	0.0496	0.0015	0.1129	0.0036	0.0165	0.0002	176	70	109	3	105	1
11	215	1.667	0.13	0.0486	0.0016	0.1109	0.0039	0.0165	0.0002	128	78	107	4	105	1
12	352	3.253	0.11	0.0485	0.0013	0.1146	0.0031	0.0171	0.0002	124	61	110	3	109	1
13	140	1.061	0.13	0.0486	0.0018	0.1115	0.0041	0.0167	0.0002	128	87	107	4	107	1
14	139	711	0.20	0.0501	0.0021	0.1107	0.0045	0.0162	0.0002	198	101	107	4	103	1
15	230	948	0.24	0.0495	0.0019	0.1127	0.0045	0.0165	0.0002	172	91	108	4	105	1
16	136	1.060	0.13	0.0467	0.0015	0.1084	0.0035	0.0168	0.0002	35	74	105	3	108	1
17	336	1.523	0.22	0.0497	0.0015	0.1160	0.0039	0.0168	0.0002	183	72	111	4	108	1
18	208	1.407	0.15	0.0471	0.0014	0.1050	0.0031	0.0161	0.0001	58	67	101	3	103	1
GT02															
1	134	170	0.79	0.0488	0.0057	0.0987	0.0110	0.0152	0.0004	139	252	96	10	97	3
2	250	265	0.94	0.0491	0.0030	0.1010	0.0059	0.0150	0.0002	154	-56	98	5	96	2
3	130	147	0.89	0.0511	0.0030	0.1029	0.0059	0.0151	0.0003	243	137	99	5	97	2
4	323	342	0.95	0.0488	0.0029	0.1036	0.0060	0.0154	0.0002	139	133	100	6	99	2
5	415	430	0.96	0.0432	0.0023	0.0921	0.0046	0.0155	0.0002			89	4	99	1
6	138	141	0.98	0.0536	0.0034	0.1111	0.0070	0.0150	0.0003	367	147	107	6	96	2
7	301	546	0.55	0.0492	0.0023	0.1032	0.0048	0.0152	0.0002	167	111	100	4	97	1
8	394	512	0.77	0.0468	0.0023	0.0965	0.0046	0.0151	0.0002	39	115	94	4	96	1
9	206	159	1.29	0.0561	0.0037	0.1170	0.0078	0.0152	0.0003	454	146	112	7	97	2
10	496	413	1.20	0.0492	0.0024	0.1021	0.0049	0.0151	0.0002	167	113	99	4	97	1
11	188	265	0.71	0.0472	0.0029	0.1004	0.0059	0.0156	0.0003	61	150	97	5	100	2
12	189	173	1.09	0.0479	0.0052	0.1005	0.0109	0.0153	0.0004	95	250	97	10	98	3
13	809	477	1.70	0.0489	0.0025	0.1029	0.0053	0.0153	0.0002	143	122	99	5	98	1
14	311	210	1.48	0.0484	0.0030	0.1023	0.0068	0.0154	0.0003	120	141	99	6	99	2
15	211	367	0.57	0.0497	0.0033	0.1014	0.0069	0.0153	0.0004	189	156	98	6	98	2
16	183	210	0.87	0.0510	0.0035	0.1067	0.0067	0.0153	0.0003	243	157	103	6	98	2

Table 2 Hafnium isotope analyses of zircons of the Late Yanshanian granites from the porphyry-skarn W-Mo deposits in the Yunkai area

Sample No.	$^{176}\text{Hf}/^{177}\text{Hf}$	$\pm(2\sigma)$	$^{176}\text{Lu}/^{177}\text{Hf}$	$^{176}\text{Yb}/^{177}\text{Hf}$	$\epsilon_{\text{Hf}}(t)$	$\pm(2\sigma)$	T_{DM1} (Ma)	$\pm(2\sigma)$	T_{DM2} (Ma)	$\pm(2\sigma)$	U-Pb points
MC10											
1	0.282 762	0.000 009	0.001 173	0.034 593	2.0	0.3	698	25	1 042	40	
2	0.282 755	0.000 009	0.001 019	0.031 951	1.7	0.3	706	25	1 058	40	
3	0.282 764	0.000 010	0.000 654	0.021 073	2.0	0.4	686	29	1 036	47	
4	0.282 756	0.000 011	0.001 494	0.040 096	1.7	0.4	713	31	1 057	49	
5	0.282 785	0.000 011	0.001 247	0.039 062	2.7	0.4	667	31	992	48	
6	0.282 772	0.000 009	0.001361	0.043 925	2.3	0.3	688	26	1 021	40	
7	0.282 783	0.000 010	0.001 472	0.048 976	2.7	0.4	674	29	996	45	
8	0.282 920	0.000 013	0.003 137	0.104 575	7.4	0.5	499	40	694	61	
9	0.282 742	0.000 012	0.000 777	0.024 034	1.3	0.4	718	33	1 085	54	
10	0.282 813	0.000 010	0.001 479	0.047 932	3.7	0.3	631	27	929	43	
11	0.282 793	0.000 009	0.001 914	0.063 648	3.0	0.3	668	25	977	39	
12	0.282 756	0.000 009	0.001 245	0.039 881	1.8	0.3	708	26	1 055	42	
13	0.282 829	0.000 011	0.002 445	0.078 825	4.2	0.4	624	32	897	49	
14	0.283 002	0.000 015	0.005 877	0.186 448	10.1	0.5	407	47	521	66	
15	0.282 778	0.000 008	0.001 269	0.040 499	4.3	0.3	678	23	958	36	
SC07											
1	0.282 621	0.000 008	0.001 751	0.052 075	-3.2	0.3	913	24	1 366	37	1
2	0.282 585	0.000 007	0.001 396	0.040 504	-4.4	0.3	955	21	1 444	33	2
3	0.282 619	0.000 008	0.001 381	0.039 415	-1.3	0.3	906	24	1 314	37	3c
4	0.282 611	0.000 006	0.001 490	0.043 578	-3.5	0.2	920	18	1 387	28	4
5	0.282 611	0.000 008	0.001 357	0.040 013	-3.5	0.3	917	24	1 387	37	5
6	0.282635	0.000009	0.001 458	0.041 999	-2.7	0.3	886	25	1 334	39	6
7	0.282 607	0.000 007	0.001 473	0.043 716	-3.7	0.2	926	19	1 396	30	7
8	0.282 626	0.000 006	0.001 723	0.050 824	-3	0.2	904	18	1 353	28	8
9	0.282 568	0.000 006	0.001 266	0.038 634	-5	0.2	976	17	1 482	27	9
10	0.282 617	0.000 008	0.001 427	0.043 266	-3.3	0.3	910	22	1 373	35	10
11	0.282 203	0.000 010	0.000 829	0.026 779	6.2	0.4	1 474	28	1 628	44	13c
12	0.282 563	0.000 007	0.001 284	0.037 851	-5.2	0.2	984	20	1 494	31	12
13	0.282 570	0.000 006	0.000 949	0.028 518	-4.9	0.2	965	16	1 476	26	11
14	0.282 615	0.000 007	0.001 758	0.051 455	-3.4	0.3	921	21	1 378	33	14
15	0.282 594	0.000 006	0.001 244	0.036 480	-4.1	0.2	939	18	1 424	28	15
SW08											
1	0.282 603	0.000 008	0.001 435	0.043 672	-4.1	0.3	930	23	1 412	37	20
2	0.282 602	0.000 008	0.001 708	0.051 302	-4.2	0.3	939	24	1 416	37	19
3	0.282 613	0.000 006	0.001433	0.043 770	-3.8	0.2	916	17	1 391	27	18
4	0.282 591	0.000 008	0.001 331	0.041 517	-4.5	0.3	945	23	1 439	37	17
5	0.281 310	0.000 010	0.000 506	0.013 333	6.4	0.4	2 678	27	2 708	43	16c
6	0.282 572	0.000 007	0.001 419	0.043 717	-5.2	0.3	974	21	1 482	33	7
7	0.282 610	0.000 007	0.000 625	0.019 498	-3.8	0.2	901	19	1 395	30	14
8	0.282 591	0.000 007	0.000 445	0.013 804	-4.5	0.2	923	19	1 437	31	13
9	0.282 617	0.000 006	0.001 470	0.045 928	-3.6	0.2	911	17	1 381	26	12
10	0.282 597	0.000 009	0.000 489	0.015 190	-4.3	0.3	916	25	1 424	40	11
11	0.282 612	0.000 008	0.000 766	0.025 093	-3.8	0.3	901	21	1 391	34	9
12	0.282 594	0.000 009	0.000 818	0.026 854	-4.4	0.3	928	24	1 431	39	6
13	0.282 599	0.000 014	0.000 790	0.024 339	-4.2	0.5	920	40	1 420	64	1
14	0.282 585	0.000 007	0.000 647	0.020 822	-4.7	0.3	936	20	1 451	32	3
15	0.282 602	0.000 008	0.000 630	0.020 282	-4.1	0.3	912	22	1 412	35	4

Table 2 Continued

Sample No.	$^{176}\text{Hf}/^{177}\text{Hf}$	$\pm(2\sigma)$	$^{176}\text{Lu}/^{177}\text{Hf}$	$^{176}\text{Yb}/^{177}\text{Hf}$	$\epsilon_{\text{Hf}}(t)$	$\pm(2\sigma)$	T_{DM1} (Ma)	$\pm(2\sigma)$	T_{DM2} (Ma)	$\pm(2\sigma)$	U-Pb points
SY03											
1	0.282 693	0.000 010	0.002 166	0.070 270	-0.6	0.3	818	28	1 205	43	
2	0.282 672	0.000 009	0.001 932	0.064 775	-1.4	0.3	844	25	1 251	39	
3	0.282 650	0.000 007	0.001 361	0.044 991	-2.1	0.3	862	21	1 298	34	
4	0.282 673	0.000 009	0.002 190	0.069 369	-1.4	0.3	848	27	1 250	41	
5	0.282 669	0.000 009	0.001 658	0.054 923	-1.5	0.3	842	27	1 257	42	
6	0.282 695	0.000 009	0.001 906	0.063 913	-0.6	0.3	810	26	1 199	40	
7	0.282 651	0.000 008	0.001 658	0.055 080	-2.1	0.3	868	24	1 298	37	
8	0.282 673	0.000 017	0.002 264	0.063 288	-1.3	0.6	849	48	1 249	74	
9	0.282 648	0.000 011	0.002 272	0.067 803	-2.3	0.4	887	32	1 307	49	
10	0.282 691	0.000 013	0.002 008	0.061 992	-0.7	0.4	818	36	1 209	56	
11	0.282 693	0.000 009	0.002 616	0.094 354	-0.7	0.3	829	26	1 207	40	
12	0.282 676	0.000 008	0.001 506	0.050 127	-1.2	0.3	828	24	1 240	38	
13	0.282 682	0.000 009	0.002 224	0.074 891	-1.0	0.3	835	27	1 228	41	
14	0.282 670	0.000 008	0.001 315	0.043 170	-1.4	0.3	832	23	1 252	36	
15	0.282 664	0.000 009	0.001 695	0.055 465	-1.6	0.3	849	26	1 267	40	
16	0.282 641	0.000 010	0.002 152	0.064 284	-2.5	0.3	893	28	1 320	44	
GT02											
1	0.282 603	0.000 011	0.000 818	0.031 138	-3.9	0.4	915	31	1 405	49	
2	0.282 597	0.000 010	0.001 222	0.048 528	-4.1	0.3	933	28	1 419	44	
3	0.282 580	0.000 011	0.001 096	0.039 525	-4.7	0.4	954	32	1 457	51	
4	0.282 624	0.000 014	0.002 593	0.074 034	-3.3	0.5	929	40	1 365	61	
5	0.282 586	0.000 010	0.000 866	0.028 874	-4.5	0.4	940	29	1 443	46	
6	0.282 591	0.000 011	0.001 069	0.038 773	-4.3	0.4	939	32	1 434	51	
7	0.282 606	0.000 009	0.001186	0.039 563	-3.8	0.3	920	26	1 399	42	
8	0.282 616	0.000 012	0.001 017	0.038 498	-3.4	0.4	901	34	1 376	54	
9	0.282 545	0.000 010	0.000 550	0.019 330	-5.9	0.4	990	29	1 534	46	
10	0.282 627	0.000 012	0.001 622	0.055 658	-3.1	0.4	901	34	1 355	53	
11	0.282 555	0.000 010	0.000 681	0.022 503	-5.6	0.3	979	27	1513	44	
12	0.282 611	0.000 011	0.001 191	0.043 718	-3.6	0.4	913	30	1 388	48	
13	0.282 578	0.000 012	0.001 538	0.044 728	-4.8	0.4	968	34	1 463	53	
14	0.282 590	0.000 009	0.001 998	0.047 894	-4.4	0.3	963	26	1 438	40	
15	0.282 576	0.000 010	0.000 930	0.030 708	-4.8	0.4	956	29	1 465	46	
16	0.282 586	0.000 009	0.001 084	0.037 465	-4.5	0.3	946	25	1 445	40	

Table 3 Sulfur isotopic compositions from porphyry-skarn W-Mo deposits in the Yunkai area

Sample	Mineral	$\delta^{34}\text{S}$ (‰)
SY01	Pyrite	+3.8
SY04	Pyrite	+3.8
SC03	Pyrite	+1.7
SC04	Pyrite	+1.2
SC06	Pyrite	+1.7
SC07	Pyrite	+1.1
SC09	Pyrrhotite	+2.4
SC11	Pyrite	+0.8
SC12	Pyrite	+2.9
SC25	Pyrite	-0.3
SC26	Pyrite	+5.2
SW07	Pyrite	+1.9

core (2 628 Ma) shows an $\epsilon_{\text{Hf}}(t)$ value of 6.4, and the calculated T_{DM2} age is 2 708 Ma.

4.3 Sulfur Isotopic Compositions

The sulfur isotope results of the sulfides in the Yunkai area are listed in Table 3. As is shown in Table 3 and Fig. 7, the value of $\delta^{34}\text{S}$ is between -0.3‰ and 5.2‰ for pyrite, the average value is 2.2‰ ($n=11$). One pyrrhotite sample shows a $\delta^{34}\text{S}$ value of 2.4‰. Galena shows $\delta^{34}\text{S}$ value between -4.2‰ and 1.0‰, and the average value is 0.9‰ ($n=7$). Sphalerite shows $\delta^{34}\text{S}$ value of 2.9‰ to 3.2‰, and the average value is 3.0‰ ($n=7$). Overall, the distribution of the $\delta^{34}\text{S}$ values in the deposits is very concentrated near zero, indicating that the sulfur was likely from a single magmatic source.

4.4 Fe Isotopic Compositions

The results of Fe isotopic compositions of pyrite are shown

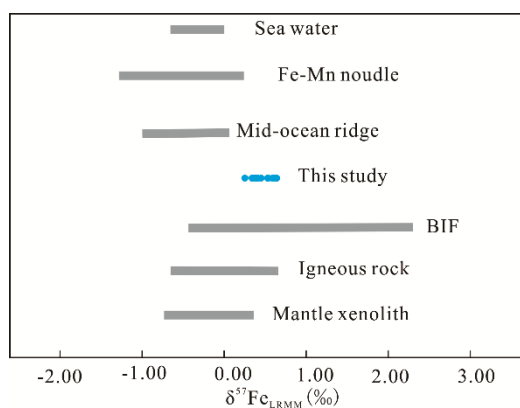


Figure 8. Iron isotope compositions comparing this study (colored symbols represent samples measured), with sea water, Fe-Mn nodule, mid-ocean ridge, BIF, igneous rock and mantle xenolith.

Table 4 Fe isotopic compositions from porphyry-skarn W-Mo deposits in the Yunkai area

Sample	$\delta^{56}\text{Fe}/^{54}\text{Fe}$	2SD	$\delta^{57}\text{Fe}/^{54}\text{Fe}$	2SD
SC-03	0.37	0.07	0.54	0.20
SC-04	0.30	0.03	0.46	0.07
SC-07	0.38	0.07	0.42	0.16
SC-09	0.22	0.11	0.35	0.12
SC-11	0.39	0.03	0.55	0.06
SC-12	0.42	0.09	0.65	0.12
SC-06	0.58	0.05	0.60	0.06
SC-25	0.16	0.08	0.26	0.08
SY-01	0.30	0.06	0.41	0.02
SY-04	0.42	0.09	0.63	0.09
SW-07	0.27	0.13	0.38	0.06

in Fig. 8 and Table 4, which show a $\delta^{56}\text{Fe}$ value from 0.16‰ to 0.58‰, with an average of 0.35‰. The $\delta^{57}\text{Fe}$ values are from 0.02‰ to 0.54‰, with an average of 0.48‰. The results show that there is no significant Fe isotopic fractionation of pyrite in different ore deposits in the Yunkai area, and value is falling in a narrow range near zero.

5 DISCUSSION

5.1 Ages for Late Yanshanian Magmatism

According to the results of LA-ICP-MS zircon U-Pb dating of granites in the Yunkai area, three stages of granitic magmatism can be distinguished: 113–110, 105–98 and 88 Ma, and all of them belong to Late Yanshanian. Together with regional tectono-magmatic evolution at the Late Mesozoic, the same periods of magmatism widely exist in South China.

Previous biotite K-Ar dating suggests the Michang granite was emplaced at 120 Ma, but our new precise LA-ICP-MS zircon U-Pb dating indicates an age of 113 ± 1 or 110 ± 1 Ma for the emplacement of this granite. In addition, the Youmapo biotite granite was also emplaced at 110 ± 1 Ma. In South China, there is a wide occurrence of ~ 110 Ma magmatic rocks. For example, the Quanzhou gabbro and adamellite from the coastal Fujian Province show emplacement ages of 111 ± 1 , 109 ± 1 and 108 ± 1 Ma (Li Z et al., 2012). The Pingtan hornblende gabbros

from southeast Fujian have an age of 115.2 ± 1.2 Ma (Dong et al., 1997). The Putuo quartz monzodiorite in the coastal Zhejiang Province shows an age of 110.2 ± 1.1 Ma (Qiu et al., 1999). The Ru'ao diabase and granite from the eastern Zhejiang Province show ages of 109.1 ± 2.8 (whole rock Ar-Ar) and 116 ± 3 Ma (SHRIMP zircon U-Pb), respectively (Dong et al., 2007).

The Longwangtang granite from Southeast Zhejiang Province shows an age of 109.8 ± 0.4 Ma (Chen et al., 1991). In addition, Xu et al. (1999) reported a Sm-Nd isochron age of 112.3 ± 17.8 Ma for a gabbroic granulite xenolith from the Qilin Cenozoic basaltic breccia pipe from Guangdong Province, suggesting an underplating of basaltic magma during this period at China's continental margin. The granites from the Michang, Sanchachong, Songwang and Youmapo deposits all show emplacement ages of 103 ± 1 , 105 ± 1 , 98 ± 1 and 103 ± 1 Ma, respectively.

Previous geochronology studies have shown that a set of I-type granite of highly calc-alkaline may exist in the southeast coastal areas during the late Early Cretaceous Period, such as the Fuzhou pluton (104 ± 5 Ma) and Danyang pluton (103 ± 10 Ma) from Fujian Province (Martin et al., 1994), the Nongliang pluton (101.2 ± 0.3 Ma) from Zhejiang Province (Chen et al., 1991). Recent studies suggest that the late Early Cretaceous Period is one of the most important tectono-magmatic events in Southeast China, and a large number of mafic to felsic magmatic rocks developed in this period, such as the Guangxi Longtuoshan rhyolitic porphyry (100.3 ± 1.4 Ma) and granite porphyry (100.3 ± 1.4 Ma) (Chen et al., 2008), the Dachang Longxianggai granite ($103\text{--}102$ Ma) (Liang et al., 2011), the mafic dykes ($110\text{--}100$ Ma) from the Northwest Jiangxi Province (Xie et al., 2002), the volcanic-intrusive rocks ($99\text{--}104$ Ma) from the western Guangdong Province (Geng et al., 2006), the mafic dykes ($103\text{--}110$ Ma) from the Northern Guangdong Province (Li et al., 1997), the granites (103 ± 1 Ma) from the Southeast Zhejiang Province (Li Y J et al., 2009), the Qingtian alkaline A-type granite (101.2 ± 2.1 Ma) and the Yandangshan volcanic rocks ($97.2\text{--}105.6$ Ma) from Zhejiang Province (Yu et al., 2006; Qiu et al., 1999), and the felsic volcanic rocks ($104\text{--}95$ Ma) in eastern Guangdong and Fujian provinces (Guo et al., 2012). In addition, there are also reports for 101 Ma mafic dyke swarm in China's southernmost Hainan Island (Tang et al., 2010).

Geochronology data show that the Late Cretaceous (~ 90 Ma) is also an important tectono-magmatic activity period in Southeast China (Fig. 9). The Songwang granite was formed during this stage (88 ± 1 Ma). The magmatic rocks emplaced during this period include: the Sheshan granite (91.1 ± 0.3 Ma) and Dachang intermediate-felsic intrusive rocks ($93\text{--}91$ Ma) in Guangxi Province (Chen et al., 2011; Cai et al., 2006); the mafic dykes ($91\text{--}88$ Ma) in northern Guangdong Province (Li et al., 1997); the basalts and the mafic dikes ($93\text{--}90$ Ma) near the Chenzhou-Ningwu fault zone in Hunan Province (Wang and Shen, 2003); the alkaline granite in Taohuadiao, Yaokeng and Daheshan, and the miarolite granite in the Putuoshan ($94\text{--}86$ Ma) in the Zhejiang Province (Xiao et al., 2007; Wang et al., 2005; Qiu et al., 1999), the alkaline granite and high-differentiation I-type granites ($96\text{--}92$ Ma) in Fujian Province (Qiu et al., 2008; Martin et al., 1994), and the Fork River

and Sanya mafic dike swarm (~93 Ma) from Hainan Island (Tang et al., 2010). In addition, SHRIMP zircon U-Pb dating of metamorphosed granite in Taiwan shows that the granite rock was originally formed in 88–87 Ma (Yui et al., 2009).

After compilation of all the available magmatic ages in Late Mesozoic (Jurassic and Cretaceous) in Southeast China, we found two significant peaks: ~100 and ~90 Ma (Fig. 9). This age distribution may suggest that there occurred two stages of strong magmatism in Southeast China during Late Yanshanian. In this paper, the granites of Michang, Youmapo, Sanchachong, and Songwang show ages of 103 and 88 Ma, corresponding to the two age peaks, indicating that the magmatic activity in the Yunkai area at Cretaceous belongs to parts of the tectono-magmatic evolution at the whole Southeast China.

5.2 Magma Source of the Late Yanshanian Granites in the Yunkai Area

Zircon Hf model ages (T_{DM2}) for the Michang biotite granite are centered on 1.3–1.2 Ga (except for one analysis), whereas the ages for the Sanchachong biotite granite and Songwang granite are slightly older at 1.5–1.3 Ga. The Michang biotite

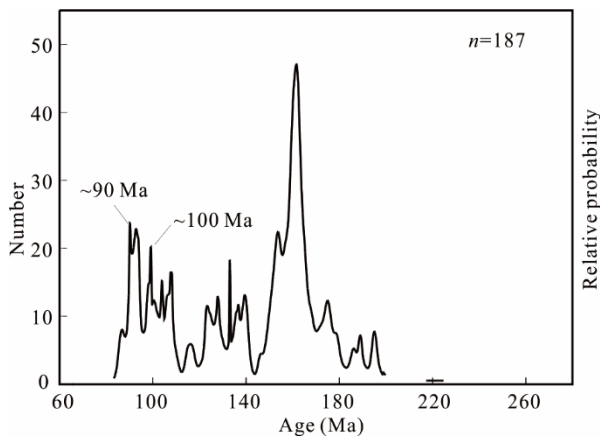


Figure 9. Histograms and cumulative probability plots of isotopic ages for Yanshanian igneous rocks in SE China (after Li et al., 2010).

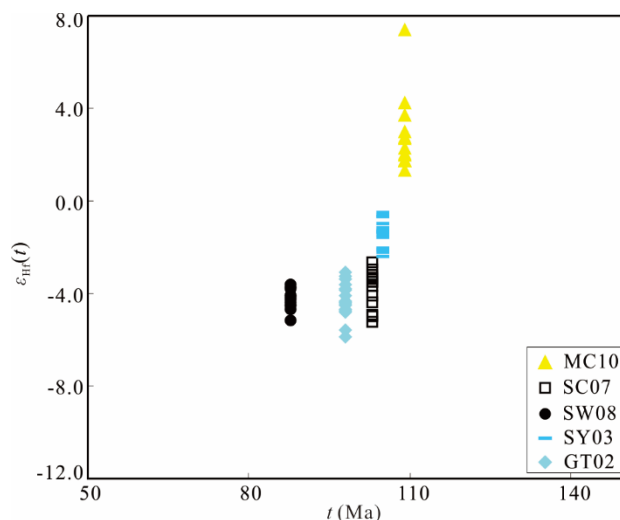


Figure 10. Relation of zircon $\epsilon_{Hf}(t)$ values versus U-Pb ages for granite samples from the porphyry-skarn W-Mo deposits in the Yunkai area.

granite contains mafic enclaves, but the rest of granites (Sanchachong, Songwang and Guandi) have no such mafic enclaves but may contain xenoliths of the country rocks. Zircons from the mafic enclaves show higher $\epsilon_{Hf}(t) > 0$, whereas those zircons from the granites show lower $\epsilon_{Hf}(t) < 0$, and there is tendency of $\epsilon_{Hf}(t)$ decrease from the Michang (110±1 Ma) to Sanchachong (103±1 Ma) and Songwang (88±1 Ma) granites (Fig. 10).

Therefore, we suggest that the Sanchachong biotite granite and Songwang granite were derived mainly from Middle Proterozoic crustal materials, whereas the Michang biotite granite may have a mantle component during magma generation.

An important question is whether there is any juvenile Proterozoic crust overgrowth at Yunkai area. Qin et al. (2006) reported a SHRIMP zircon U-Pb age of 1 462±28 Ma for the plagioclase amphibolite from the Yunkai Group in Southeast Guangxi Province, which is interpreted as metamorphosed OIB-type mafic volcanic rocks, suggesting the existence of juvenile Proterozoic mafic crust in Yunkai area. Gilder et al. (1996) reported Nd model ages of 1.4±0.3 Ga for 23 Mesozoic granites in South China, and they also suggested occurrence of a wide range of Proterozoic crust in South China. Wang and Shen (2003) used the Nd model ages of granites in the Southeast China as well as the U-Pb ages of inherited zircons in the crustal rocks to suggest an episodic crustal growth characteristic in Southeast China, and the Middle Proterozoic (~1.4 Ga) is one of the most important stages for the crustal growth. It is also important to note that a number of 1.3–1.4 Ga detrital zircon with positive $\epsilon_{Hf}(t)$ values and younger T_{DM2} are found from the Neoproterozoic sedimentary rocks in the Southern Yangtze Block and the Cathysia Block (including the Wuyi Mountain, Nanling, Yunkai areas), which also indicates existence of Middle Proterozoic crust in South China (Liu et al., 2010; Wang D H et al., 2010; Yu et al., 2010, 2008). All the above evidence indicates the existence of the juvenile Middle Proterozoic crusts in South China including the Yunkai area, therefore it is suggested that these crustal materials may provide an important source for the magmatic rocks of Late Yanshanian in this region.

The existence of mafic enclaves in the Michang biotite granite indicates contribution of mantle-derived magma and its interaction with crustal derived felsic magma, which is also supported by the zircon Hf isotope data which show a relatively higher $\epsilon_{Hf}(t)$ values and young two-stage model Hf T_{DM2} age for the Michang biotite granite and its mafic enclaves than the other granites in the district (Fig. 10). In addition, there also exists one positive $\epsilon_{Hf}(t)$ value (1.4) for zircon from the biotite granite, which is similar to the $\epsilon_{Hf}(t)$ values (1.3–10.1) for the mafic enclaves, indicating an magma mixing process for the generation of the granitic magma. The mantle-derived magma can also provide deep heat for the middle and lower crust material to partial melting to generate granite magma.

5.3 Source of the Ore-Forming Materials in the Yunkai Area

Sulfides from the ore deposits show a small $\delta^{34}S$ variation around zero, which may indicate that the sulfur source was derived from the single magmatic fluid. Together with sulfur isotope data from previous studies (e.g., Fu et al., 2014), all the ores

of skarn-type and quartz vein-type show consistent sulfur isotopic composition with a narrow range close to zero. This $\delta^{34}\text{S}$ range indicates that the sulfur of all these skarn- and vein-type deposits was derived from a single source related to magmatic hydrothermal fluid with the H_2S as the dominant species (Ohmoto and Rye, 1979; Ohmoto, 1972). The sulfide minerals are mainly pyrite, chalcopyrite and molybdenite, without sulfate minerals. To trace the sulfur source, we need to apply the total sulfur isotopic composition ($\delta^{34}\text{S}_\Sigma$) of the hydrothermal fluids during sulfide precipitation. When H_2S predominates in the fluid system, under the condition of equilibrium, $\delta^{34}\text{S}_\Sigma \approx \delta^{34}\text{S}_{\text{fluid}} \approx \delta^{34}\text{S}_{\text{pyrite}}$, as a result, the near zero $\delta^{34}\text{S}$ value indicates that the sulfur source is single in the main metallogenic precipitation period, possibly from deep-sourced magma. Therefore, the mineralization in the Youmapo tungsten-molybdenum deposit, Sanchachong tungsten deposit and Songwang tungsten-tin deposit has a close relationship with the Late Yanshanian magmatism.

Iron isotope system is a newly developed non-traditional isotope system that has already been applied in solving a variety of geologic problems including ore genesis. As iron is one of the major metallogenic elements, iron isotopic geochemistry can provide a new tracer for the mineralization, which has shown its important role in tracing the source of ore-forming materials and fluids, the fluid evolution, the supergene alteration and other important mineralization processes, such as the BIF (Dauphas et al., 2004; Johnson et al., 2003), Precambrian stratiform sulfide deposits (Zhu et al., 2008), the Archean komatiite-hosted Ni deposits (Bekker et al., 2009), the Archaean quartz-conglomerate-type gold deposits (Hofmann et al., 2009), the modern ocean floor hydrothermal systems (Sharma, 2001), and the porphyry and skarn-type deposits (Wang Y et al., 2011; Graham et al., 2004). All these studies indicate that the iron isotope has a great potential in tracing the ore-forming mechanism.

The three typical porphyry and skarn-type deposits of Sanchachong, Youmapo and Songwang show identical Fe isotopic compositions of pyrite near zero. This Fe isotope characteristic may suggest the source of iron in the deposits may be derived from magma, which is in support from the sulfur isotope data as we discussed above. Therefore, the mineralization is closely related to magmatism.

5.4 Late Yanshanian W-Mo Mineralization Event

The mineralization age for the porphyry and skarn-type deposit is generally close to the age of related granites, therefore we can date the ore-related magmatic rocks to indirectly constrain the metallogenic epoch. For example, the Cu-Au-Mo-related granodioritic porphyries from the porphyry and skarn-type ore deposits at Jiurui District, Jiangxi Province show zircon U-Pb ages between 138.2±1.8 and 148.0±1.0 Ma (Jiang et al., 2013; Xu et al., 2013, 2012; Yang et al., 2011; Li and Jiang, 2009; Ding et al., 2005), which are identical to the molybdenite Re-Os ages of 137.9±1.0 and 146.4±2.6 Ma (Li et al., 2007; Wu and Zou, 1997). In the Dexing porphyry-type Cu deposit, Zhou et al. (2012) obtained molybdenite Re-Os ages of 170.4±1.8 to 172.3±2.3 Ma, which are also similar to the ages (170.2±0.9 to 172.5±0.5 Ma) of ore-bearing porphyry (Liu et al., 2012). Taking all the zircon U-Pb age data in the Yunkai area in Guangxi Province, the Michang, Sanchachong and

Songwang granites show ages of 113, 103 and 88 Ma, therefore it is reasonable to estimate that the Michang skarn-type tungsten-molybdenum deposit, the Sanchachong skarn-type tungsten-molybdenum deposit and the Songwang porphyry molybdenum-tungsten deposit were all formed during the Late Cretaceous (80–110 Ma).

In South China, multiple stages of tectonic-magmatic events produced polycyclic magmatic rocks and associated Cu-Au-Pb-Zn-Ag and W-Sn-Mo mineralizations (Li and Jiang, 2016; Li et al., 2016; Xu et al., 2015; Jiang et al., 2013, 2008, 2006; Guo et al., 2012; Mao et al., 2011, 2008; Wang and Shen, 2003). Most of the granites were emplaced in a cyclic manner during the Caledonian, Indosinian and Yanshanian periods (Hua et al., 2013). The Yunkai area is a typical area in South China where developed typical Caledonian movement, which produced large Caledonian granites, and lots of the mineralization in this district have a close genetic relation with the Caledonian granites. For example, Chen et al. (2011) reported Caledonian ages for the Sheshan biotite granodiorite and the Shedong tungsten-molybdenum deposit (437.8 Ma). Li X et al. (2012) reported zircon SHRIMP U-Pb age of 429.6±4.3 Ma for the biotite granite and scheelite Sm-Nd isochron age of 431±12 Ma for the Niutangjie skarn-type tungsten deposit. In recent years, a number of Indosinian W-Sn-Mo deposits have been found in the Yunkai area and its adjacent regions, such as the Li Guifu tungsten-tin deposit (213.3±2.9 Ma, Zhou et al., 2009) and the Yuntoujie W-Mo deposit (213.3±2.9 Ma, Wu et al., 2012).

It is worth attention that in the Yunkai area, the Michang tungsten-molybdenum deposit, the Sanchachong tungsten-molybdenum deposit, the Youmapo tungsten-molybdenum deposit and the Songwang molybdenum-tungsten deposit were all formed during Late Yanshanian stage of magmatism and mineralization (Late Cretaceous). Combined all available data, it is clear that the Yunkai area which is located in the southwest side of the Qinhang metallogenic belt developed the Late Cretaceous magmatic rocks (80–100 Ma) and related tungsten-molybdenum-copper (gold) deposits (Table 5). Li et al. (2008) obtained a molybdenite Re-Os isochron age of 95.4±1.0 Ma for the Damingshan tungsten deposit in Guangxi Province and molybdenite Re-Os model ages of 95.0–95.8 Ma for the Maling tungsten deposit, which is similar to the white mica $^{39}\text{Ar}/^{40}\text{Ar}$ ages (97.1±0.8, 98.0±1.0 Ma). In the Guangxi Longtoushan gold deposits, the ore-bearing granitic porphyry has emplacement ages of 96.1±3 to 100.3±1.4 Ma (Duan et al., 2011; Chen et al., 2008), which are similar to the Pingtianshan intrusive rocks (96.2±0.4 Ma) in the area. In the Dayaoshan area, the granite porphyry related to the Baoshan porphyry copper deposit shows an emplacement age of 91.1±0.6 Ma (Bi et al., 2015). All these data suggest existence of a wide range of Late Yanshanian magmatism and mineralization in the Yunkai area.

Late Yanshanian W-Sn and Cu-Au polymetallic mineralizations are widely distributed in the southeast coast, Southwest Yunnan and Guangxi provinces and other regions in South China. Among them, the metallogenic epoch of the W-Sn deposits in West Yunnan and Guangxi provinces are mostly concentrated in Late Cretaceous, in agreement with the magmatic emplacement ages. For example, Wang et al. (2005) reported fluid inclusions

Table 5 Representative geochronology ages of Late Cretaceous magmatic rocks (80–100 Ma) and related W-Mo-(Sn-Cu) mineralization in South China

Locality	Rock type	Age (Ma)	Method	Reference
Yandangshan	Felsic volcanic rock	97±2, 99±4, 106±4	SHRIMP U-Pb	Yu et al. (2006)
Quanzhou	Gabbro and adamellite	111±1, 109±1, 108±1	SHRIMP U-Pb	Li Z et al. (2012)
Eastern Guangdong and Fujian	Felsic volcanic rocks	104–95	LA-ICPMS U-Pb	Guo et al. (2012)
Northern Guangdong	Mafic dykes	91–88		Li et al. (1997)
Dachang	Porphyritic granite, Q-diorite porphyrite	91±1	SHRIMP U-Pb	Cai et al. (2006)
Longtoushan	Rhyolite	103±2	SHRIMP U-Pb	Chen et al. (2008)
Pingtian	Biotite granite	125±1	TIMS U-Pb	Dong et al. (1997)
Damingshan tungsten deposit	Molybdenite	95.4±1.0	Re-Os	Li et al. (2008)
Maling tungsten deposit	Molybdenite	95.0 to 95.8	Re-Os	Li et al. (2008)
Longtoushan gold deposits	White mica	97.1±0.8, 98.0±1.0	³⁹ Ar/ ⁴⁰ Ar	Chen et al. (2008)
Longtoushan gold deposits	Ore-bearing granitic porphyry	96.1±3, 100.3±1.4	LA-ICPMS U-Pb	Duan et al. (2011)
Baoshan porphyry copper deposit	Ore-bearing granitic porphyry	91.1±0.6	LA-ICPMS U-Pb	Bi et al. (2015)
Dachang tin-polymetallic deposit	Fluid inclusions	91.4±2.9, 94.5±0.3, 94.6±0.5	³⁹ Ar/ ⁴⁰ Ar	Wang D H et al. (2010)
Dachang tin-polymetallic deposit	Sericite and phlogopite	77.4±0.6, 95.3±0.7	³⁹ Ar/ ⁴⁰ Ar	Cheng et al. (2013)
Chenzhou-Ningwu fault zone	Basalts and the mafic dykes	93–90		Wang and Shen (2003)
Northwest Jiangxi	Mafic dykes	110–100	LA-ICPMS U-Pb	Xie et al. (2002)
Northern Tailuko belt	Meta-granite	87±1, 88±2	SHRIMP U-Pb	Yui et al. (2009)
Kafang deposit	Molybdenite	83.4±2.1	Re-Os	Mao et al. (2008)
Putuoshan	Alkaine granite	94±1	TIMS U-Pb	Qiu et al. (1999)
Taohuadiao	Alkaine granite	93±1	TIMS U-Pb	Qiu et al. (1999)
Eastern Zhejiang	Confucianism diabase	109±3	Whole rock Ar-Ar	Dong et al. (2007)
Eastern Zhejiang	Granite	116±3	SHRIMP U-Pb	Dong et al. (2007)
Shipingchuan	K-feldspar granite	103±1	LA-ICPMS U-Pb	Li Y J et al. (2009)
Qingtian	Alkaline granite	101±2	TIMS U-Pb	Qiu et al. (1999)
Daheshan	Quartz syenite	86±3	SHRIMP U-Pb	Wang et al. (2005)
Yaokeng	K-feldspar granite	91±3	LA-ICPMS U-Pb	Xiao et al. (2007)
Diaocun	Granodiorite	104±3	LA-ICPMS U-Pb	Geng et al. (2006)
Kuiqi	Alkaline granite	96–92	Rb-Sr	Martin et al. (1994)
Dacengshan	Granite	93±2	LA-ICPMS U-Pb	Qiu et al. (2008)
Dajing	K-feldspar granite	94±2	LA-ICPMS U-Pb	Qiu et al. (2008)
Nanzhen	K-feldspar granite	96±3	LA-ICPMS U-Pb	Qiu et al. (2008)
Sansha	Granite	92±2	LA-ICPMS U-Pb	Qiu et al. (2008)

³⁹Ar/⁴⁰Ar ages of 91.4±2.9, 94.5±0.3 and 94.6±0.5 Ma for the Dachang tin-polymetallic deposit in Guangxi Province. Cheng et al. (2013) reported sericite and phlogopite ³⁹Ar/⁴⁰Ar ages of 77.4±0.6 to 95.3±0.7 Ma for the Yunnan Gejiu Sn-W deposits in Yunnan Province, which are similar to the molybdenite Re-Os age (83.4±2.1 Ma) in the Kafang deposit. In the southeast coastal region, a number of hypabyssal type low temperature hydrothermal copper-gold-silver deposits also formed at around 100 Ma (Mao et al., 2008).

Therefore, it is suggested that magmatism and mineralization are widely developed in this area during Late Cretaceous Period, and the magmatic rocks and W-Mo-Cu-Au deposits occur not only in continental margin coastal areas in South China, but also in the inland regions such as the Yunkai area, which has significant implications in finding Late Yanshanian mineralization and those closely related magmatism in the Yunkai area.

6 CONCLUSIONS

(1) A wide range of magmatism and mineralization in the Yunkai area of South China occur during the Late Yanshanian Period.

(2) Zircon U-Pb ages of the ore-bearing biotite granites

and their mafic enclaves from the newly discovered Michang, Youmapo, Sanchachong and Songwang porphyry-skarn W-Mo deposits are from 88±1 to 110±1 Ma.

(3) Hf isotopic compositions of granitic zircons show negative $\epsilon_{\text{Hf}}(t)$ values of -5.9 to -0.6, with calculated Hf model age (T_{DM2}) of 1.5–1.2 Ga, indicating that the Middle Proterozoic crustal materials may have provided an important source for the magmatic rocks in this district during the Late Yanshanian Period.

(4) Sulfur and iron isotopes of the sulfides from the porphyry-skarn type W-Sn-Mo deposits in the Yunkai area indicate that the ore-forming materials may come from the deep-sourced granitic magma, and the mineralizations show a close relationship with the granitic magmatism during the Late Yanshanian Period.

ACKNOWLEDGMENTS

This work was supported by the Fundamental Research Funds for the Central Universities (No. CUG120702). The final publication is available at Springer via <https://doi.org/10.1007/s12583-017-0901-1>.

REFERENCES CITED

- Bekker, A., Barley, M. E., Fiorentini, M. L., et al., 2009. Atmospheric Sulfur in Archean Komatiite-Hosted Nickel Deposits. *Science*, 326(5956): 1086–1089. <https://doi.org/10.1126/science.1177742>
- Bi, S. J., Yang, Z., Li, W., et al., 2015. Discovery of Late Cretaceous Bao-shan Porphyry Copper Deposit in Dayaoshan, Qinhang Metallogenic Belt: Constraints from Zircon U-Pb Age and Hf Isotope. *Earth Science—Journal of China University of Geosciences*, 40(9): 1458–1479 (in Chinese with English Abstract)
- Blichert-Toft, J., Chauvel, C., Albarède, F., 1997. Separation of Hf and Lu for High-Precision Isotope Analysis of Rock Samples by Magnetic Sector-Multiple Collector ICP-MS. *Contributions to Mineralogy and Petrology*, 127(3): 248–260. <https://doi.org/10.1007/s004100050278>
- Cai, M. H., He, L. Q., Liu, G. Q., et al., 2006. SHRIMP Zircon U-Pb Dating of the Intrusive Rocks in the Dachang Tin-Polymetallic Ore Field, Guangxi and Their Geological Significance. *Geological Review*, 52(3): 409–414 (in Chinese with English Abstract)
- Chen, C. H., Liu, Y. H., Lee, C. Y., et al., 2012. Geochronology of Granulite, Charnockite and Gneiss in the Poly-Metamorphosed Gaozhou Complex (Yunkai Massif), South China: Emphasis on the In-Situ EMP Monazite Dating. *Lithos*, 144–145: 109–129. <https://doi.org/10.1016/j.lithos.2012.04.009>
- Chen, F. W., Li, H. Q., Mei, Y. P., 2008. Zircon SHRIMP U-Pb Chronology of Mineralization of the Longtoushan Porphyry Gold Orefield, Gui County, Guangxi. *Acta Geologica Sinica*, 82(7): 921–926 (in Chinese with English Abstract)
- Chen, J. F., Zhou, T. X., Yin, C. S., 1991. ^{40}Ar - ^{39}Ar Dating of Several Mesozoic Plutons in Southeastern Zhejiang Province. *Acta Petrologica Sinica*, 7(3): 37–44 (in Chinese with English Abstract)
- Chen, M. H., Mo, C. S., Huang, Z. Z., et al., 2011. Zircon LA-ICP-MS U-Pb Ages of Granitoid Rocks and Molybdenite Re-Os Age of Shedong W-Mo Deposit in Cangwu County of Guangxi and Its Geological Dignificance. *Mineral Deposits*, 30(6): 963–978 (in Chinese with English Abstract)
- Chen, Y. C., Pei, R. F., Zhang, H. L., 1990. The Geology of Nonferrous and Rare Metal Deposits Related to Mesozoic Granitoids in the Nanling Region, China. *Acta Geoscientica Sinica*, 20(1):79–85 (in Chinese with English Abstract)
- Cheng, Y. B., Mao, J. W., Chang, Z. S., et al., 2013. The Origin of the World Class Tin-Polymetallic Deposits in the Gejiu District, SW China: Constraints from Metal Zoning Characteristics and ^{40}Ar - ^{39}Ar Geochronology. *Ore Geology Reviews*, 53(2): 50–62. <https://doi.org/10.1016/j.oregeorev.2012.12.008>
- Dauphas, N., Van, Z. M., Wadhwa, M., et al., 2004. Clues from Fe Isotope Variations on the Origin of Early Archean BIFs from Greenland. *Science*, 306(5704): 2077–2080. <https://doi.org/10.1126/science.1104639>
- Deng, X. G., Chen, Z. G., Li, X. H., et al., 2004. SHRIMP U-Pb Zircon Dating of the Darongshan-Shiwandashan Granitoid Belt in Southeastern Guangxi, China. *Geological Review*, 50(4): 426–432 (in Chinese with English Abstract)
- Ding, X., Jiang, S. Y., Zhao, K. D., et al., 2005. In-Situ U-Pb SIMS Dating and Trace Element (EMPA) Composition of Zircon from a Granodiorite Porphyry in the Wushan Copper Deposit, China. *Mineralogy and Petrology*, 86(1/2): 29–44. <https://doi.org/10.1007/s00710-005-0093-5>
- Dong, C. W., Xu, X. S., Yan, Q., et al., 2007. A New Case of Late Mesozoic Crust-Mantle Interaction in Eastern Zhejiang: Geochronology and Geochemistry of the Ru'ao Diabase-Granite Composite Intrusions. *Acta Petrologica Sinica*, 23(6): 1303–1312 (in Chinese with English Abstract)
- Dong, C. W., Zhou, X. M., Li, H. M., et al., 1997. Late Mesozoic Crust-Mantle Interaction in Southeastern Fujian. *Chinese Science Bulletin*, 42(6): 495–498. <https://doi.org/10.1007/bf02882602>
- Duan, R. C., Ling, W. L., Li, Q., et al., 2011. Correlations of the Late Yanshanian Tectonomagmatic Events with Metallogenesis in South China: Geochemical Constraints from the Longtoushan Gold Ore Deposit of the Dayaoshan Area, Guangxi Province. *Acta Geologica Sinica*, 85(10):1644–1658 (in Chinese with English Abstract)
- Fu, Q., Ge, W. S., Wen, C. S., et al., 2011. Geochemistry and Genesis of Michang Granites and Their Dark Microgranular Enclaves in Guangxi. *Acta Geoscientica Sinica*, 32(3): 293–303 (in Chinese with English Abstract)
- Fu, Q., Ge, W. S., Wen, C. S., et al., 2014. Geochemistry and Genesis of Youmapo W-Mo Deposit in Guangxi. *Mineral Deposits*, 33(4): 785–794 (in Chinese with English Abstract)
- Geng, H. Y., Xu, X. S., O'Reilly, S. Y., et al., 2006. Cretaceous Volcanic-Intrusive Magmatism in Western Guangdong and Its Geological Significance. *Science in China Series D: Earth Sciences*, 49(7): 696–713. <https://doi.org/10.1007/s11430-006-0696-7>
- GGST (Guangxi Geology Survey Team), 1986. Reports on 1 : 50 000 Regional Geological Surveys of Yulin, Longsheng, Shatian, Michang. Report of Guangxi Geology Survey Team, Nanning (in Chinese)
- Gilder, S. A., Gill, J., Coe, R. S., et al., 1996. Isotopic and Paleomagnetic Constraints on the Mesozoic Tectonic Evolution of South China. *Journal of Geophysical Research: Solid Earth*, 101(B7): 16137–16154. <https://doi.org/10.1029/96jb00662>
- Graham, S., Pearson, N., Jackson, S., et al., 2004. Tracing Cu and Fe from Source to Porphyry: In Situ Determination of Cu and Fe Isotope Ratios in Sulfides from the Grasberg Cu-Au Deposit. *Chemical Geology*, 207(3/4): 147–169. <https://doi.org/10.1016/j.chemgeo.2004.02.009>
- Griffin, W. L., Pearson, N. J., Belousova, E., et al., 2000. The Hf Isotope Composition of Cratonic Mantle: LAM-MC-ICPMS Analysis of Zircon Megacrysts in Kimberlites. *Geochimica et Cosmochimica Acta*, 64(1): 133–147
- Griffin, W. L., Wang, X., Jackson, S. E., et al., 2002. Zircon Chemistry and Magma Mixing, SE China: In Situ Analysis of Hf Isotopes, Tonglu and Pingtan Igneous Complexes. *Lithos*, 61(3–4): 237–269. [https://doi.org/10.1016/S0024-4937\(02\)00082-8](https://doi.org/10.1016/S0024-4937(02)00082-8)
- Guo, F., Fan, W. M., Li, C. W., et al., 2012. Multi-Stage Crust-Mantle Interaction in SE China: Temporal, Thermal and Compositional Constraints from the Mesozoic Felsic Volcanic Rocks in Eastern Guangdong-Fujian Provinces. *Lithos*, 150(7): 62–84. <https://doi.org/10.1016/j.lithos.2011.12.009>
- Hofmann, A., Bekker, A., Rouxel, O., et al., 2009. Multiple Sulphur and Iron Isotope Composition of Detrital Pyrite in Archaean Sedimentary Rocks: A New Tool for Provenance Analysis. *Earth and Planetary Science Letters*, 286(3/4): 436–445. <https://doi.org/10.1016/j.epsl.2009.07.008>
- Hu, Z. C., Gao, S., Liu, Y. S., et al., 2008a. Signal Enhancement in Laser Ablation ICP-MS by Addition of Nitrogen in the Central Channel Gas. *Journal of Analytical Atomic Spectrometry*, 23(8): 1093–1101. <https://doi.org/10.1039/b804760j>
- Hu, Z. C., Liu, Y. S., Gao, S., et al., 2008b. A Local Aerosol Extraction Strategy for the Determination of the Aerosol Composition in Laser Ablation Inductively Coupled Plasma Mass Spectrometry. *Journal of Analytical Atomic Spectrometry*, 23(9): 1192–1203. <https://doi.org/10.1039/b803934h>
- Hu, Z. C., Liu, Y. S., Gao, S., et al., 2012a. Improved In Situ Hf Isotope Ratio Analysis of Zircon Using Newly Designed X Skimmer Cone and Jet Sample Cone in Combination with the Addition of Nitrogen by Laser Ablation Multiple Collector ICP-MS. *Journal of Analytical Atomic Spectrometry*, 27(9): 1391–1399. <https://doi.org/10.1039/C2JA30078H>
- Hu, Z. C., Liu, Y. S., Gao, S., et al., 2012b. A “Wire” Signal Smoothing Device for Laser Ablation Inductively Coupled Plasma Mass Spectro-

- metry Analysis. *Spectrochimica Acta Part B Atomic Spectroscopy*, 78: 50–57. <https://doi.org/10.1016/j.sab.2012.09.007>
- Hua, R. M., Zhang, W. L., Chen, P. R., et al., 2013. Relationship between Caledonian Granitoids and Large-Scale Mineralization in South China. *Geological Journal of China Universities*, 19(1): 1–11 (in Chinese with English Abstract)
- Jiang, S. Y., Xu, R. M., Zhu, Z. Y., et al., 2013. Study on Mesozoic Tectonics and Granitic Magmatism and Their Relationship with Cu-Au Mineralization in the Jiurui Ore District, Jiangxi Province. *Acta Petrologica Sinica*, 29(12): 4051–4068 (in Chinese with English Abstract)
- Jiang, S. Y., Zhao, K. D., Jiang, Y. H., et al., 2006. A New Type of Tin Mineralization Related to Granite in South China: Evidence from Mineral Chemistry, Element and Isotope Geochemistry. *Acta Petrologica Sinica*, 22(10): 2509–2516 (in Chinese with English Abstract)
- Jiang, S. Y., Zhao, K. D., Jiang, Y. H., et al., 2008. Characteristics and Genesis of Mesozoic A-Type Granites and Associated Mineral Deposits in the Southern Hunan and Northern Guangxi Provinces along the Shi-Hang Belt, South China. *Geological Journal of China Universities*, 14: 283–294 (in Chinese with English Abstract)
- Johnson, C. M., Beard, B. L., Beukes, N. J., et al., 2003. Ancient Geochemical Cycling in the Earth as Inferred from Fe Isotope Studies of Banded Iron Formations from the Transvaal Craton. *Contributions to Mineralogy & Petrology*, 144(5): 523–547. <https://doi.org/10.1007/s00410-002-0418-x>
- Li, B., Jiang, S. Y., Zhang, Q., et al., 2016. Geochemistry, Geochronology and Sr-Nd-Pb-Hf Isotopic Compositions of Middle to Late Jurassic Syenite-Granodiorites-Dacite in South China: Petrogenesis and Tectonic Implications. *Gondwana Research*, 35: 217–237. <https://doi.org/10.13039/501100001809>
- Li, J. W., Li, X. H., Pei, R. F., et al., 2007. Re-Os Age of Molybdenite from the Southern Ore Zone of the Wushan Copper Deposit, Jiangxi Province, and Its Geological Significance. *Acta Geologica Sinica*, 81(6): 801–807 (in Chinese with English Abstract)
- Li, L., Jiang, S. Y., 2009. Petrogenesis and Geochemistry of the Dengjiashan Porphyritic Granodiorite, Jiujiang-Ruichang Metallogenic District of the Middle-Lower Reaches of the Yangtze River. *Acta Petrologica Sinica*, 25: 2877–2888 (in Chinese with English Abstract)
- Li, Q., Duan, R. C., Ling, W. L., et al., 2009. Detrital Zircon U-Pb Geochronology of the Early Paleozoic Strata in Eastern Guangxi and Its Constraint on the Caledonian Tectonic Nature of the Cathaysian Continental Block. *Earth Science—Journal of China University of Geosciences*, 34(1): 189–202 (in Chinese with English Abstract)
- Li, Q., Jiang, S. Y., 2016. Trace and Rare Earth Element Characteristics in Fe-Mn Carbonates Associated with Stratiform Ag-Pb-Zn Mineralization from the Lengshuikeng Ore District, Jiangxi Province: Implications for Their Genesis and Depositional Environment. *Journal of Earth Science*, 27(4): 571–583. <https://doi.org/10.1007/s12583-016-0908-9>
- Li, S. R., Wang, D. H., Liang, T., et al., 2008. Metallogenic Epochs of the Damingshan Tungsten Deposit in Guangxi and Its Prospecting Potential. *Acta Geologica Sinica*, 82(7): 873–879 (in Chinese with English Abstract)
- Li, X., Feng, Z., Xiao, R., et al., 2012. Spatial and Temporal Distributions and the Geological Setting of the W-Sn Mo-Nb-Ta Deposits at the Northeast Guangxi, South China. *Acta Geologica Sinica*, 86(11): 1713–1725 (in Chinese with English Abstract)
- Li, X. H., Hu, R. Z., Rao, B., 1997. Geochronology and Geochemistry of Cretaceous Mafic Dikes from Northern Guangdong, SE China. *Geochimica*, 26(2): 14–31 (in Chinese with English Abstract)
- Li, X. H., Li, W. X., Wang, X. C., et al., 2010. SIMS U-Pb Zircon Geochronology of Porphyry Cu-Au-(Mo) Deposits in the Yangtze River Metallogenic Belt, Eastern China: Magmatic Response to Early Cretaceous Lithospheric Extension. *Lithos*, 119(3/4): 427–438. <https://doi.org/10.1016/j.lithos.2010.07.018>
- Li, Y. J., Wei, J. H., Yao, C. L., et al., 2009. Zircon U-Pb Dating and Tectonic Significance of the Shipingchuan Granite in Southeastern Zhejiang Province, SE China. *Geological Review*, 55(5): 673–684 (in Chinese with English Abstract)
- Li, Z., Qiu, J. S., Xu, X. S., 2012. Geochronological, Geochemical and Sr-Nd-Hf Isotopic Constraints on Petrogenesis of Late Mesozoic Gabbro-granite Complexes on the Southeast Coast of Fujian, South China: Insights into a Depleted Mantle Source Region and Crust-Mantle Interactions. *Geological Magazine*, 149(3): 459–482. <https://doi.org/10.1017/s0016756811000793>
- Li, Z. X., Li, X. H., 2007. Formation of the 1 300-km-Wide Intracontinental Orogen and Postorogenic Magmatic Province in Mesozoic South China: A Flat-Slab Subduction Model. *Geology*, 35(2): 179. <https://doi.org/10.1130/g23193a.1>
- Li, Z. X., Li, X. H., Wartho, J. A., et al., 2009. Magmatic and Metamorphic Events during the Early Paleozoic Wuyi-Yunkai Orogeny, Southeastern South China: New Age Constraints and Pressure-Temperature Conditions. *Geological Society of America Bulletin*, 122(5/6): 772–793. <https://doi.org/10.1130/b30021.1>
- Liang, T., Wang, D. H., Hou, K. J., et al., 2011. LA-MC-ICP-MS Zircon U-Pb Dating of Longxianggai Pluton in Dachang of Guangxi and Its Geological Significance. *Acta Petrologica Sinica*, 27(6): 1624–1636 (in Chinese with English Abstract)
- Ling, H. F., Shen, W. Z., Sun, T., et al., 2006. Genesis and Source Characteristics of 22 Yanshanian Granites in Guangdong Province: Study of Element and Nd-Sr Isotopes. *Acta Petrologica Sinica*, 22(11): 2687–2703 (in Chinese with English Abstract)
- Liu, R., Zhou, H. W., Zhang, L., et al., 2010. Zircon U-Pb Ages and Hf Isotope Compositions of the Mayuan Migmatite Complex, NW Fujian Province, Southeast China: Constraints on the Timing and Nature of a Regional Tectonothermal Event Associated with the Caledonian Orogeny. *Lithos*, 119(3/4): 163–180. <https://doi.org/10.1016/j.lithos.2010.06.004>
- Liu, S., Wang, D., Chen, Y., et al., 2008. $^{40}\text{Ar}/^{39}\text{Ar}$ Ages of Muscovite from Different Types Tungsten-Bearing Quartz Veins in the Chong-Yu-You Concentrated Mineral Area in Gannan Region and Its Geological Significance. *Acta Geologica Sinica*, 82(7): 932–940 (in Chinese with English Abstract)
- Liu, X., Fan, H. R., Santosh, M., et al., 2012. Remelting of Neoproterozoic Relict Volcanic Arcs in the Middle Jurassic: Implication for the Formation of the Dexing Porphyry Copper Deposit, Southeastern China. *Lithos*, 150(10): 85–100. <https://doi.org/10.1016/j.lithos.2012.05.018>
- Ludwig, K. R., 2003. Isoplot/EX Version 3.0, A Geochronological Toolkit for Microsoft Excel. Berkeley Geochronology Center Special Publication, Berkeley
- Mao, J. W., Chen, M. H., Yuan, S. D., et al., 2011. Geological Characteristics of the Qinhang (or Shihang) Metallogenic Belt in South China and Spatial-Temporal Distribution Regularity of Mineral Deposits. *Acta Geologica Sinica*, 85(5): 636–658 (in Chinese with English Abstract)
- Mao, J. W., Xie, G. Q., Guo, C. L., 2008. Spatial-Temporal Distribution of Mesozoic Ore Deposits in South China and Their Metallogenic Settings. *Geological Journal of China Universities*, 14(4): 510–526 (in Chinese with English Abstract)
- Martin, H., Bonin, B., Capdevila, R., et al., 1994. The Kuiqi Peralkaline Granitic Complex (SE China): Petrology and Geochemistry. *Journal of*

- Petrology*, 35(4): 983–1015. <https://doi.org/10.1093/petrology/35.4.983>
- Ohmoto, H., 1972. Systematics of Sulfur and Carbon Isotopes in Hydrothermal Ore Deposits. *Economic Geology*, 67(5): 551–578. <https://doi.org/10.2113/gsecongeo.67.5.551>
- Ohmoto, H., Rye, R. O., 1979. Isotopes of Sulfur and Carbon. In: Barnes, H. L., ed., *Geochemistry of Hydrothermal Ore Deposits*. Wiley-Interscience, New York. 509–567
- Peng, S. B., Jin, Z. M., Fu, J. M., et al., 2006. The Geochemical Evidences and Tectonic Significance of Neoproterozoic Ophiolite in Yunkai District, Western Guangdong Province, China. *Acta Geologica Sinica*, 80(6): 814–825 (in Chinese with English Abstract)
- Qin, X. F., Pan, Y. M., Li, J., et al., 2006. Zircon SHRIMP U-Pb Geochronology of the Yunkai Metamorphic Complex in Southeastern Guangxi, China. *Geological Bulletin of China*, 25(5): 553–559 (in Chinese with English Abstract)
- Qiu, J. S., Wang, D. Z., McInnes, B. I. A., 1999. Geochemistry and Petrogenesis of the I- and A-Type Composite Granite Masses in the Coastal Area of Zhejiang and Fujian Provinces. *Acta Petrologica Sinica*, 15(2): 237–246 (in Chinese with English Abstract)
- Qiu, J. S., Xiao, E., Hu, J., et al., 2008. Petrogenesis of Highly Fractionated I-Type Granites in the Coastal Area of Northeastern Fujian Province: Constraints from Zircon U-Pb Geochronology, Geochemistry and Nd-Hf Isotopes. *Acta Petrologica Sinica*, 24(11): 2468–2484 (in Chinese with English Abstract)
- Scherer, E., Muenker, C., Mezger, K., 2001. Calibration of the Lutetium-Hafnium Clock. *Science*, 293(5530): 683–687. <https://doi.org/10.1126/science.1061372>
- Segal, I., Halicz, L., Platzner, I. T., 2003. Accurate Isotope Ratio Measurements of Ytterbium by Multiple Collection Inductively Coupled Plasma Mass Spectrometry Applying Erbium and Hafnium in an Improved Double External Normalization Procedure. *Journal of Analytical Atomic Spectrometry*, 18(10): 1217–1223. <https://doi.org/10.1039/b307016f>
- Sharma, R., 2001. Indian Deep-Sea Environment Experiment (Index): A Study for Environmental Impact of Deep Seabed Mining in Central Indian Ocean. *Deep-Sea Research II*, 48: 3295–3426
- Tang, L. M., Chen, H. L., Dong, C. W., et al., 2010. Late Mesozoic Tectonic Extension in SE China: Evidence from the Basic Dike Swarms in Hainan Island, China. *Acta Petrologica Sinica*, 26(4): 1204–1216 (in Chinese with English Abstract)
- Tang, Y. L., 2009. Geological Characteristics and Ore Controlling Factors of the Songwang W-Sn-Mo Deposit in Bobai County, Guangxi Province. *Mineral Resources and Geology*, 23(2): 158–162 (in Chinese)
- Wan, Y. S., Liu, D. Y., Wilde, S. A., et al., 2010. Evolution of the Yunkai Terrane, South China: Evidence from SHRIMP Zircon U-Pb Dating, Geochemistry and Nd Isotope. *Journal of Asian Earth Sciences*, 37(2): 140–153. <https://doi.org/10.1016/j.jseaes.2009.08.002>
- Wang, D. H., Chen, Y. C., Chen, W., et al., 2010. Dating of the Dachang Superlarge Tin-Polymetallic Deposit in Guangxi and Its Implication for the Genesis of the No. 100 Orebody. *Acta Geologica Sinica—English Edition*, 78(2): 452–458. <https://doi.org/10.1111/j.1755-6724.2004.tb00153.x>
- Wang, D. Z., Shen, W. Z., 2003. Genesis of Granitoids and Crustal Evolution in Southeast China. *Earth Science Frontiers*, 10(3): 209–220 (in Chinese with English Abstract)
- Wang, L. J., Griffin, W. L., Yu, J. H., et al., 2010. Precambrian Crustal Evolution of the Yangtze Block Tracked by Detrital Zircons from Neoproterozoic Sedimentary Rocks. *Precambrian Research*, 177(1/2): 131–144. <https://doi.org/10.1016/j.precamres.2009.11.008>
- Wang, Q., Zhao, Z. H., Jian, P., et al., 2005. Geochronology of Cretaceous A-Type Granitoids or Alkaline Intrusive Rocks in the Hinterland, South China: Constraints from Late Mesozoic Tectonic Evolution. *Acta Petrologica Sinica*, 21(3): 795–808 (in Chinese with English Abstract)
- Wang, Y., Zhu, X. K., Mao, J. W., et al., 2011. Iron Isotope Fractionation during Skarn-Type Metallogeny: A Case Study of Xinqiao Cu-S-Fe-Au Deposit in the Middle-Lower Yangtze Valley. *Ore Geology Reviews*, 43(1): 194–202. <https://doi.org/10.1016/j.oregeorev.2010.12.004>
- Wang, Y. J., Fan, W. M., Zhang, G. W., et al., 2013. Phanerozoic Tectonics of the South China Block: Key Observations and Controversies. *Gondwana Research*, 23(4): 1273–1305. <https://doi.org/10.13039/501100002367>
- Wang, Y. J., Fan, W. M., Zhao, G. C., et al., 2007. Zircon U-Pb Geochronology of Gneissic Rocks in the Yunkai Massif and Its Implications on the Caledonian Event in the South China Block. *Gondwana Research*, 12(4): 404–416. <https://doi.org/10.1016/j.gr.2006.10.003>
- Wang, Y. J., Wu, C. M., Zhang, A. M., et al., 2012. Kwangsi and Indosinian Reworking of the Eastern South China Block: Constraints on Zircon U-Pb Geochronology and Metamorphism of Amphibolites and Granulites. *Lithos*, 150(5): 227–242. <https://doi.org/10.1016/j.lithos.2012.04.022>
- Wang, Y. J., Zhang, A. M., Fan, W. M., et al., 2011. Kwangsi Crustal Anatexis within the Eastern South China Block: Geochemical, Zircon U-Pb Geochronological and Hf Isotopic Fingerprints from the Gneissoid Granites of Wugong and Wuyi-Yunkai Domains. *Lithos*, 127(1/2): 239–260. <https://doi.org/10.13039/501100001809>
- Wiedenbeck, M., Alle, P., Corfu, F., et al., 1995. Three Natural Zircon Standards for U-Th-Pb, Lu-Hf, Trace Element and REE Analyses. *Geostandards Newsletter*, 19(1): 1–23. <https://doi.org/10.1111/j.1751-908X.1995.tb00147.x>
- Woodhead, J., Hergt, J., Shelley, M., et al., 2004. Zircon Hf-Isotope Analysis with an Excimer Laser, Depth Profiling, Ablation of Complex Geometries, and Concomitant Age Estimation. *Chemical Geology*, 209(1/2): 121–135. <https://doi.org/10.1016/j.chemgeo.2004.04.026>
- Wu, J., Liang, H. Y., Huang, W. T., et al., 2012. Indosinian Isotope Ages of Plutons and Deposits in Southwestern Miaoershan-Yuechengling, Northeastern Guangxi and Implications on Indosinian Mineralization in South China. *Chinese Science Bulletin*, 57(9): 1024–1035 (in Chinese)
- Wu, L. S., Zou, X. Q., 1997. Re-Os Isotopic Age Study of the Chengmenshan Copper Deposit, Jiangxi Province. *Mineral Deposits*, 16(4): 376–381 (in Chinese with English Abstract)
- Xiao, E., Qiu, J. S., Xu, X. S., et al., 2007. Geochronology and Geochemistry of the Yaokeng Alkaline Granitic Pluton in Zhejiang Province: Petrogenetic and Tectonic Implications. *Acta Petrologica Sinica*, 23(6): 1431–1440 (in Chinese with English Abstract)
- Xie, G. Q., Hu, R. Z., Jia, D. C., 2002. Geological and Geochemical Characteristics and Its Significance of Mafic Dikes from Northwest Jiangxi Province. *Geochimica*, 31(4): 329–337 (in Chinese with English Abstract)
- Xu, B., Jiang, S. Y., Wang, R., et al., 2015. Late Cretaceous Granites from the Giant Dulong Sn-Polymetallic Ore District in Yunnan Province, South China: Geochronology, Geochemistry, Mineral Chemistry and Nd-Hf Isotopic Compositions. *Lithos*, 218–219: 54–72. <https://doi.org/10.1016/j.lithos.2015.01.004>
- Xu, X. S., Zhou, X. M., O'Reilly, Y. S., et al., 1999. Genesis of Granitoids and Crustal Evolution in Southeast China. *Acta Petrologica Sinica*, 15(2): 217–223 (in Chinese with English Abstract)
- Xu, Y. M., Jiang, S. Y., Zhu, Z. Y., et al., 2012. Geochronology, Geochemistry and Mineralization of the Quartz Diorite-Porphyrite and Granodiorite Porphyry in the Shanshangwan Area of the Jiurui Ore District, Jiangxi Province. *Acta Petrologica Sinica*, 28(10): 3306–3324 (in Chi-

- nese with English Abstract)
- Xu, Y. M., Jiang, S. Y., Zhu, Z. Y., et al., 2013. Geochronology, Geochemistry and Mineralogy of Ore-Bearing and Ore-Barren Intermediate-Acid Intrusive Rocks from the Jiurui Ore District, Jiangxi Province and Their Geological Implications. *Acta Petrologica Sinica*, 29(12): 4291–4310 (in Chinese with English Abstract)
- Yang, S. Y., Jiang, S. Y., Li, L., et al., 2011. Late Mesozoic Magmatism of the Jiurui Mineralization District in the Middle-Lower Yangtze River Metallogenic Belt, Eastern China: Precise U-Pb Ages and Geodynamic Implications. *Gondwana Research*, 20(4): 831–843. <https://doi.org/10.1016/j.gr.2011.03.012>
- Yang, Z., Liu, R., Wang, X., et al., 2014. Petrogenesis and Tectonic Significance of Late Yanshanian Granites in the Yunkai Area, Southeast China: Evidence from Zircon U-Pb Ages and Lu-Hf Isotopes. *Earth Science—Journal of China University of Geosciences*, 39(9): 1258–1276 (in Chinese with English Abstract)
- Ye, Z. G., 2005. Geological Characteristics and Ore Controlling Factors of the Sanchachong W Deposit in Bobai County, Guangxi Province. *Land and Resources of Southern China*, 12: 31–34 (in Chinese)
- Yu, J. H., O'Reilly, S. Y., Wang, L. J., et al., 2008. Where was South China in the Rodinia Supercontinent?. *Precambrian Research*, 164(1/2): 1–15. <https://doi.org/10.1016/j.precamres.2008.03.002>
- Yu, J. H., O'Reilly, S. Y., Wang, L. J., et al., 2010. Components and Episodic Growth of Precambrian Crust in the Cathaysia Block, South China: Evidence from U-Pb Ages and Hf Isotopes of Zircons in Neoproterozoic Sediments. *Precambrian Research*, 181(1–4): 97–114. <https://doi.org/10.1016/j.precamres.2010.05.016>
- Yu, M. G., Xing, G. F., Shen, J. L., et al., 2006. Chronologic Study on Volcanic Rocks in the Mt. Yandangshan World Geopark. *Acta Geologica Sinica*, 80(11): 1683–1690 (in Chinese with English Abstract)
- Yui, T. F., Okamoto, K., Usuki, T., et al., 2009. Late Triassic–Late Cretaceous Accretion/Subduction in the Taiwan Region along the Eastern Margin of South China—Evidence from Zircon SHRIMP Dating. *International Geology Review*, 51(4): 304–328. <https://doi.org/10.1080/00206810802636369>
- Zhang, F. F., Wang, Y. J., Zhang, A. M., et al., 2012. Geochronological and Geochemical Constraints on the Petrogenesis of Middle Paleozoic (Kwanghsian) Massive Granites in the Eastern South China Block. *Lithos*, 150(5): 188–208. <https://doi.org/10.1016/j.lithos.2012.03.011>
- Zhao, K. D., Jiang, S. Y., Jiang, Y. H., et al., 2006. SHRIMP U-Pb Dating of the Furong Unit of Qitangling Granite from Southeast Hunan Province and Their Geological Implications. *Acta Petrologica Sinica*, 22(10): 2611–2616 (in Chinese with English Abstract)
- Zhao, K. D., Jiang, S. Y., Yang, S. Y., et al., 2012. Mineral Chemistry, Trace Elements and Sr-Nd-Hf Isotope Geochemistry and Petrogenesis of Cailing and Furong Granites and Mafic Enclaves from the Qitianling Batholith in the Shi-Hang Zone, South China. *Gondwana Research*, 22(1): 310–324. <https://doi.org/10.1016/j.gr.2011.09.010>
- Zhong, K. B., Huang, F. Y., 2007. Geological Characteristics and Prospecting Potential of the Michang W-Mo Deposit in Luchuan County, Guangxi Province. *Land and Resources of Southern China*, 9: 27–31 (in Chinese)
- Zhou, Q., Jiang, Y. H., Liao, S. Y., et al., 2012. SHRIMP Zircon U-Pb Dating and Hf Isotope Studies of the Doroite Porphyrite from the Dexing Copper Deposit. *Acta Geologica Sinica*, 86(11): 1726–1734 (in Chinese with English Abstract)
- Zhou, X. M., Sun, T., Shen, W. Z., et al., 2006. Petrogenesis of Mesozoic Granitoids and Volcanic Rocks in South China: A Response to Tectonic Evolution. *Episodes*, 29(1): 26–33
- Zhou, X. W., Cui, S. Q., Wen, J., et al., 2009. Re-Os Isotope Dating of the Liguifu Tungsten-Tin Polymetallic Deposit in Dupangling Area, Guangxi. *Geology in China*, 36(4): 837–844 (in Chinese with English Abstract)
- Zhou, Y. Z., Zhen, Y., Zeng, C. Q., et al., 2015. On the Understanding of Qinzhou Bay-Hangzhou Bay Metallogenic Belt, South China. *Earth Science Frontiers*, 22(2): 1–6 (in Chinese with English Abstract)
- Zhu, X. K., Li, Z. H., Tang, S. H., et al., 2008. Fe Isotope Characteristics of Early Precambrian Pyrite Deposits and Their Geological Significance: Examples from Shandong and Hebei Provinces. *Acta Petrologica et Mineralogica*, 27(5): 429–434 (in Chinese with English Abstract)